J|A|C|S ARTICLES

Published on Web 08/07/2009

Peroxo-Type Intermediates in Class I Ribonucleotide Reductase and Related Binuclear Non-Heme Iron Enzymes

Kasper P. Jensen,[†] Caleb B. Bell, III,[‡] Michael D. Clay,[‡] and Edward I. Solomon*[,‡]

Department of Chemistry, Stanford University, 333 Campus Drive, Mudd Building, Stanford, California 94305-5080, and DTU-Chemistry, Technical University of Denmark, Building 207, DK 2800 Kgs. Lyngby, Denmark

Received December 22, 2008; E-mail: edward.solomon@stanford.edu

Abstract: We have performed a systematic study of chemically possible peroxo-type intermediates occurring in the non-heme di-iron enzyme class Ia ribonucleotide reductase, using spectroscopically calibrated computational chemistry. Density functional computations of equilibrium structures, Fe−O and O−O stretch frequencies, Mössbauer isomer shifts, absorption spectra, *J*-coupling constants, electron affinities, and free energies of O_2 and proton or water binding are presented for a series of possible intermediates. The results enable structure−property correlations and a new rationale for the changes in carboxylate conformations occurring during the O_2 reaction of this class of non-heme iron enzymes. Our procedure identifies and characterizes various possible candidates for peroxo intermediates experimentally observed along the ribonucleotide reductase dioxygen activation reaction. The study explores how water or a proton can bind to the di-iron site of ribonucleotide reductase and facilitate changes that affect the electronic structure of the iron sites and activate the site for further reaction. Two potential reaction pathways are presented: one where water adds to Fe1 of the cis-μ-1,2 peroxo intermediate P causing opening of a bridging carboxylate to form intermediate P′ that has an increased electron affinity and is activated for proton-coupled electron transfer to form the Fe(III)Fe(IV) intermediate X; and one that is more energetically favorable where the P to P′ conversion involves addition of a proton to a terminal carboxylate ligand in the site which increases the electron affinity and triggers electron transfer to form X. Both pathways provide a mechanism for the activation of peroxy intermediates in binuclear non-heme iron enzymes for reactivity. The studies further show that water coordination can induce the conformational changes observed in crystal structures of the met state.

Introduction

Metalloproteins perform complex biochemical tasks with high specificity and efficiency.[1] One case of complex chemistry is the controlled use of otherwise highly reactive radicals to initiate molecular conversions in proteins.[2] An important example of such radical chemistry is oxygen atom removal from RNA building blocks, ribonucleoside diphosphates, to yield corresponding DNA building blocks, deoxyribonucleoside diphosphates, by ribonucleotide reductases (RNR).[3] Three classes of proteins have evolved to perform this task, and all three are distinct types of metalloproteins. Class I RNRs contain two iron atoms in one part of the protein, the R2 subunit, which is separated from the catalytic site in the R1 subunit where the radical chemistry involving the ribonucleotide occurs.[4]

Dioxygen binds to the biferrous site to form a peroxo intermediate, which is converted into a strongly oxidizing intermediate (X) upon reduction by an exogenous electron. This intermediate can then abstract a hydrogen atom from a near-by tyrosine residue in the protein. The resulting tyrosine radical is subsequently responsible for accepting an electron over a distance of ∼35 Å from a cysteine in the catalytic site of the R1 subunit,[5] thereby allowing the resulting cysteine radical to initiate the reaction that leads to deoxyribonucleotides. Understanding the molecular events between binding of O_2 to iron and generation of the essential oxidizing intermediate X is a key question for understanding oxygen-activation in RNR and other, similar, binuclear non-heme iron enzymes.

In the deoxy state of Class I RNR, the site consists of two Fe(II) ions each bound to one histidine and one terminal acidic residue, with Asp-84 (*Escherichia coli* numbering is used throughout) binding to Fe1 and Glu-204 binding to Fe2 (see Figure 1).[6] Two Glu residues form μ-1,3 bridges between the two iron atoms. This architecture is common in O_2-activating non-heme di-iron enzymes, other examples being methane monooxygenase (MMO) and stearoyl-acyl carrier protein Δ^9 desaturase (Δ^9D).[7−9]

[†] DTU-Chemistry.
[‡] Department of Chemistry, Stanford University.

(1) Karlin, K. D. *Science* **1993**, *261*, 701–708.
(2) Stubbe, J.; Van der Donk, W. A. *Chem. Rev.* **1998**, *98*, 705–762.
(3) Reichard, P. *Science* **1993**, *260*, 1773–1777.
(4) Nordlund, P.; Reichard, P. *Annu. Rev. Biochem.* **2006**, *75*, 681–706.
(5) Uhlin, U.; Eklund, H. *Nature* **1994**, *370*, 533–539.
(6) Nordlund, P.; Sjoberg, B. M.; Eklund, H. *Nature* **1990**, *345*, 593–598.
(7) Holm, R. H.; Kennepohl, P.; Solomon, E. I. *Chem. Rev.* **1996**, *96*, 2239–2314.
(8) Solomon, E. I.; Brunold, T. C.; Davis, M. I.; Kemsley, J. N.; Lee, S.-K.; Lehnert, N.; Neese, F.; Skulan, A. J.; Yang, Y.-S.; Zhou, J. *Chem. Rev.* **2000**, *100*, 235–350.
(9) Wallar, B. J.; Lipscomb, J. D. *Chem. Rev.* **1996**, *96*, 2625–2657.

10.1021/ja809983g CCC: $40.75

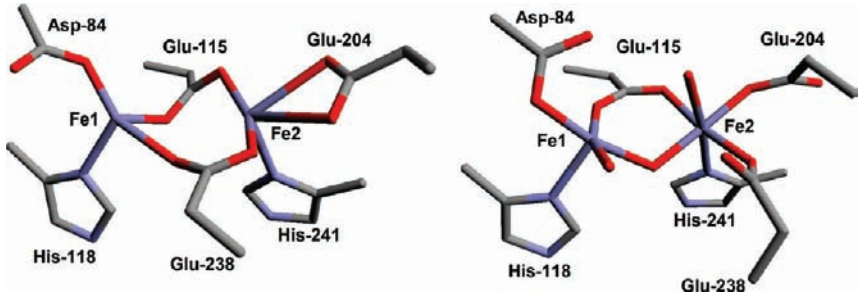

Figure 1. Deoxy (4C,5C) and met (5C,6C) forms of class Ia ribonucleotide reductase.[10,16] Note in the met structure that three new oxygen atoms are present, two terminal and one bridging; these come from dioxygen and a water molecule that add to the site during the reaction.

In recent structures of reduced deoxy wild-type (WT) RNR from *E. coli*, at pH 5 and 7.3,[10] both the terminal acidic residues are in a syn conformation with respect to iron, with Asp-84 clearly monodentate. Magnetic circular dichroism (MCD) studies have shown that the deoxy state consists of a 4-coordinate and a 5-coordinate iron center.[11] Consequently, Glu-204 is bidentate, which implies that water may bind to the empty coordination site on 4-coordinate Fe1 early on the reaction coordinate.[12]

Mutation of Asp-84 to a glutamate, to provide a ligand environment similar to that found in MMO, renders this residue bidentate, which is in accordance with MCD data, and Glu-204 becomes monodentate.[13] The RNR mutant, however, remains distinct from MMO, which has a μ-1,1 type Glu-bridge, most likely due to the effects of second sphere residues.[13] The structures suggest that carboxylate conformational changes constitute an important aspect of these enzymes[14,15] and underscores the need to investigate the mechanistic relevance of such carboxylate conformations.

Since crystal structures of the final diferric form of the protein also exist, it is possible to compare the structural differences between the diferrous, reduced, and the diferric, or met, state (Figure 1).[16] Notable changes, which must occur in addition to O_2-binding and electron transfer during the intermediate steps, include: (i) binding of one water molecule to the site; (ii) a shift of Glu-238 from bridging to terminal, monodentate coordination to Fe2, and hydrogen bonding to a solvent molecule on Fe1 (either the incoming water molecule or an oxygen atom derived from reductive cleavage of O_2); and (iii) switching of terminal Glu-204 coordinating to Fe2 from a syn-conformation in the reduced state to an anti conformation in the met (i.e., oxidized) state. The carboxylates are expected[17] and computed[18] to be quite flexible, partly explaining the disorder in the crystals. The starting point of this study was the idea that these structural changes have to be incorporated into a so far unknown detailed mechanism of oxygen activation,[19,20] which may be relevant for RNR, and a variety of non-heme di-iron proteins.

As the first step of the oxygen activation mechanism, it is assumed that O_2 binds to the ferrous deoxy state to form a diferric peroxo-intermediate (P). Such an intermediate has been observed in the D84E mutant RNR,[21] the W48F/D84E double mutant RNR,[22] Δ^9D,[23] MMO,[24,25] and WT mouse RNR,[26] but not in WT *E. coli* RNR. These peroxo-intermediates appear similar in chemical structure, with Mössbauer isomer shifts of ca. 0.66 ± 0.02 mm/s in Δ^9D[27] and 0.63 mm/s in mouse RNR[26] and in the D84E mutant of RNR.[28] The data are consistent with a μ-1,2 geometry of the coordinating peroxide.[21,29] Since structural data are not directly available for intermediates between the deoxy state and met state, the detailed structures of these intermediates are not known, and computations serve an important role in providing the necessary atomistic detail; such computations have been consistent with a μ-1,2 geometry,[29,30] whereas for MMO, an μ-η^2,η^2 geometry has been suggested.[31]

An additional intermediate has recently been observed in the RNR W48A/Y122F double mutant, which falls between P and X in the oxygen activation pathway and must be very short-lived in WT RNR.[32] The removal of Trp-48 eliminates the electron transfer (ET) required to produce X, and chemical rescue experiments that restore this ability directly produce X from this intermediate. This observation has substantial impor-

(10) Voegtli, W. C.; Sommerhalter, M.; Saleh, L.; Baldwin, J.; Bollinger, J. M., Jr.; Rosenzweig, A. C. *J. Am. Chem. Soc.* **2003**, *125*, 15822–15830.
(11) Yang, Y.-S.; Baldwin, J.; Ley, B. A.; Bollinger, Jr., J. M.; Solomon, E. I. *J. Am. Chem. Soc.* **2000**, *122*, 8495–8510.
(12) Calhoun, J. R.; Bell, C. B., III; Smith, T. J.; Thamann, T. J.; DeGrado, W. F.; Solomon, E. I. *J. Am. Chem. Soc.* **2008**, *130*, 9188–9189.
(13) Wei, P.-P.; Skulan, A. J.; Mitic, N.; Yang, Y.-S.; Saleh, L.; Bollinger, J. M., Jr.; Solomon, E. I. *J. Am. Chem. Soc.* **2004**, *126*, 3777–3788.
(14) Kolberg, M.; Strand, K. R.; Graff, P.; Andersson, K. K. *Biochim. Biophys. Acta* **2004**, *1699*, 1–34.
(15) Strand, K. R.; Karlsen, S.; Kolberg, M.; Røhr, Å. K.; Görbitz, H. C.; Andersson, K. K. *J. Biol. Chem.* **2004**, *279*, 46794–46801.
(16) Hogbom, M.; Galander, M.; Andersson, M.; Kolberg, M.; Hofbauer, W.; Lassmann, G.; Nordlund, P.; Lendzian, F. *Proc. Natl. Acad. Sci. U.S.A.* **2003**, *100*, 3209–3214.
(17) Lee, D.; Lippard, S. J. *Inorg. Chem.* **2002**, *41*, 2704–2719.
(18) Torrent, M.; Musaev, D. G.; Morokuma, K. *J. Phys. Chem.* **2001**, *105*, 322–327.
(19) Rardin, R. L.; Tolman, W. B.; Lippard, S. J. *New J. Chem.* **1991**, *15*, 417–430.
(20) Que, Jr., L.; Dong, Y. *Acc. Chem. Res.* **1996**, *29*, 190–196.
(21) Moenne-Loccoz, P.; Baldwin, J.; Ley, B.; Loehr, T.; Bollinger, J. *Biochemistry* **1998**, *37*, 14659–14663.
(22) Baldwin, J.; Voegtli, W.; Khidekel, N.; Moenne-Loccoz, P.; Krebs, C.; Pereira, A.; Ley, B.; Huynh, B.; Loehr, T.; Riggs-Gelasco, P.; Rosenzweig, A.; Bollinger, J. *J. Am. Chem. Soc.* **2001**, *123*, 7017–7030.
(23) Broadwater, J. A.; Ai, J. Y.; Loehr, T. M.; Sanders-Loehr, J.; Fox, B. G. *Biochemistry* **1998**, *37*, 14664–14671.
(24) Lee, S.; Lipscomb, J. *Biochemistry* **1999**, *38*, 4423–4432.
(25) Valentine, A.; Stahl, S.; Lippard, S. *J. Am. Chem. Soc.* **1999**, *121*, 3876–3887.
(26) Yun, D.; Garcia-Serres, R.; Chicalese, B. M.; Na, Y. H.; Huynh, B. H.; Bollinger, J. M., Jr. *Biochemistry* **2007**, *46*, 1925–1932.
(27) Broadwater, J. A.; Achim, C.; Munck, E.; Fox, B. G. *Biochemistry* **1999**, *38*, 12197–12204.
(28) Bollinger, J. M.; Krebs, C.; Vicol, A.; Chen, S. X.; Ley, B. A.; Edmondson, D. E.; Huynh, B. H. *J. Am. Chem. Soc.* **1998**, *120*, 1094–1095.
(29) Skulan, A. J.; Brunold, T. C.; Baldwin, J.; Saleh, L.; Bollinger, J. M., Jr.; Solomon, E. I. *J. Am. Chem. Soc.* **2004**, *126*, 8842–8855.
(30) Wei, P.-P.; Skulan, A. J.; Wade, H.; DeGrado, W. F.; Solomon, E. I. *J. Am. Chem. Soc.* **2005**, *127*, 16098–16106.
(31) Gherman, B. F.; Baik, M.-H.; Lippard, S. J.; Friesner, R. A. *J. Am. Chem. Soc.* **2004**, *126*, 2978–2990.
(32) Saleh, L.; Krebs, C.; Ley, B. A.; Naik, S.; Huynh, B. H.; Bollinger, J. M., Jr. *Biochemistry* **2004**, *43*, 5953–5964.

Table 1. Experimental Data for Intermediates P and P′ in RNR-Proteins

	Fe−O[a]/ cm^{-1}	O−O[b]/ cm^{-1}	J[c]/ cm^{-1}	δ[d]/ mms^{-1}	λ[e]/ cm^{-1}	ε[f]/ M^{-1} cm^{-1}
P in RNR D84E				0.63/0.63[28]	14 000[28]	1500[28]
P in RNR W48F/ D84E	457[21,29]	868[21,29]	−50[35]	0.65/0.61[35]	14 000[22]	1800[22]
P in mouse RNR				0.63/0.63[26]		
P′ in RNR W48A/ Y122F				0.52/0.52	32 000[32]	1300[32]
				0.45/0.45 or 0.45/0.60 0.43/0.43[32]	(20 000)	(100)

[a] Fe−O stretch frequency from resonance Raman spectroscopy. [b] O−O stretch frequency from resonance Raman spectroscopy. [c] Exchange coupling constant from Mössbauer spectroscopy. [d] Isomer shifts of irons Fe1/Fe2. [e] Position of peak of maximum absorption in UV−vis spectra. [f] Corresponding extinction coefficients.

tance for the reaction, in terms of setting the stage for the reductive formation of X, the ultimate oxidant of Tyr-122, and thus for understanding the general mechanism of oxygen activation. This intermediate, which will be referred to here as P′, has Mössbauer isomer shifts in-between intermediates P (0.63 mm/s) and X (0.26 and 0.56 mm/s),[33] interpreted as arising from two ferric species in thermal equilibrium because the ratio of two these species does not change during the formation of P′.[32] In one interpretation, two symmetric diferric species have δ = 0.45 mm/s and δ = 0.52 mm/s in a 3:1 thermal mixture.[32] Alternatively, one of the species could be asymmetric with δ = 0.45 mm/s and δ = 0.60 mm/s, whereas the other species would have δ = 0.43 mm/s.[32] Furthermore, the characteristic electronic transition of P at 700 nm ($\varepsilon \approx 1800$ M^{-1} cm^{-1})[30] has been replaced in P′ by a transition at 310 nm ($\varepsilon \approx 1300$ M^{-1} cm^{-1}) and a very weak feature at ca. 500 nm ($\varepsilon \approx 100$ M^{-1} cm^{-1})[32] which implies structural changes to the peroxo moiety. However, since the W48A variation, which trapped this species, eliminates the extra electron and Mössbauer shows both irons are in the ferric oxidation state, the O−O bond must still be intact. Interestingly, an intermediate with high similarity to P′ has recently been observed in toluene/o-xylene monooxygenase (ToMO).[34] This species has no absorption spectrum, an isomer shift of 0.55 mm/s and appears to react directly with phenol.[34] The experimental properties of P and P′ intermediates are summarized in Table 1.

The generation of X from P′ requires at least an exogenous electron from a donor, which in class Ia RNR could be a small protein such as YfaE or NrdF.[36,37] This electron is transferred via Trp-48 to P′, which is then converted into X. X subsequently abstracts a hydrogen from Tyr-122 to form the Tyr radical and the diferric state observed in the met crystal structure. A schematic representation of the identified intermediates in the RNR reaction is given in Figure 2.[2]

The aim of the present study is to investigate chemically possible structures and the associated physical and spectroscopic

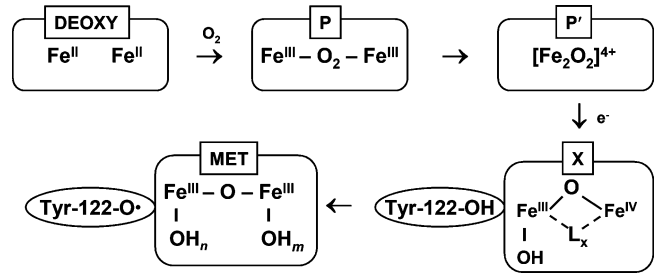

Figure 2. Schematic representation of states observed in the class Ia ribonucleotide reductase O_2 reaction.

properties of peroxo intermediates in RNR. Computational chemistry allows comparisons, in atomistic detail, with high relative accuracy. In these considerations, it is important to use structural and spectroscopic experimental data as constraints. The structure of the met state has three oxygen atoms in the iron site, requiring that a water molecule be bound in addition to the two oxygen atoms from O_2 at some point along the reaction coordinate. At the same time, changes in carboxylate coordination modes are enigmatic[19] and require mechanistic consideration. Also, proton transfer would likely be associated with the reduction of the peroxy intermediate for charge neutrality and should occur along the reaction coordinate. Similarly, the isomer shifts constrain the reaction coordinate in terms of electronic structure, as do UV−vis absorption features, Raman data, and J-coupling constants, both from protein and model complexes.[38] In addition, given the uncertainties in computational procedures, the computed free energies of the candidate intermediates should be reasonable and consistent with the overall scope of the reaction coordinate.

Four types of peroxy structures are considered: (1) species where only O_2 is bound to the crystalographically defined deoxy site; (2) structures where H_2O is bound to one iron subsequent to O_2 binding; (3) structures where the coordinated water in (2) is allowed to dissociate to OH^- and H^+; and (4) structures where O_2 and a proton from solvent are bound to the deoxy state. The results of these model calculations are then correlated to the experimental data on P and P′ to elucidate the activation of the peroxide for reduction in the reaction mechanism of RNR.

Methodology

Computational Details. The calculations were carried out with the Turbomole program,[39] version 5.8. The Becke 1988 exchange and Perdew 1986 nonlocal correlation functionals (BP86)[40,41] were used for computation of structures, energies, and properties. Theoretical studies of transition metal systems have had a long history of calibration and development,[42−44] with typical accuracies of ca. 0.03 Å for metal−ligand bond lengths and mean absolute errors of 50 kJ/mol for reaction energies (metal ligand bond dissociation energies).[45] Energies involving substantial changes in orbital occupation and thus correlation effects[46] display larger errors. Using a functional such as BP86 for first-row transition metals is in accordance with current consensus.[45,46]

(33) Sturgeon, B. E.; Burdi, D.; Chen, S.; Huynh, B.-H.; Edmondson, D. E.; Stubbe, J.; Hoffman, B. M. *J. Am. Chem. Soc.* **1996**, *118*, 7551–7557.
(34) Murray, L. J.; Naik, S. G.; Ortillo, D. O.; Garcia-Serres, R.; Lee, J. K.; Huynh, B. H.; Lippard, S. J. *J. Am. Chem. Soc.* **2007**, *129*, 14500–14510.
(35) Krebs, C.; Bollinger, J. M., Jr.; Theil, E. C.; Huynh, B. H. *J. Biol. Inorg. Chem.* **2002**, *7*, 863–869.
(36) Wu, C. H.; Jiang, W.; Krebs, C.; Stubbe, J. A. *Biochemistry* **2007**, *46*, 11577–11588.
(37) Jordan, A.; Reichard, P. *Annu. Rev. Biochem.* **1998**, *67*, 71–98.
(38) Tshuva, E. Y.; Lippard, S. J. *Chem. Rev.* **2004**, *104*, 987–1012.
(39) Alrichs, R.; Bär, M.; Häser, M.; Horn, H.; Kölmel, C. *Chem. Phys. Lett.* **1989**, *162*, 165–169.
(40) Becke, A. D. *Phys. Rev. A* **1988**, *38*, 3098–3100.
(41) Perdew, J. P. *Phys. Rev. B* **1986**, *33*, 8822–8824.
(42) Ziegler, T. *Chem. Rev.* **1991**, *91*, 651–667.
(43) Siegbahn, P. E. M.; Blomberg, M. R. A. *Chem. Rev.* **2000**, *100*, 421–437.
(44) Frenking, G.; Frohlich, N. *Chem. Rev.* **2000**, *100*, 717–774.
(45) Jensen, K. P.; Roos, B. O.; Ryde, U. *J. Chem. Phys.* **2007**, *126*, 014103.
(46) Neese, F. *J. Biol. Inorg. Chem.* **2006**, *11*, 702–711.

The basis sets used for geometry optimization were def2-SVP for all atoms,[47] a recent double-ζ all-polarizable basis set which is parametrized to give a balanced description of the elements in the periodic table and is thus particularly suitable for transition metal systems. All optimizations were carried out in redundant internal coordinates. Fully unrestricted calculations were performed for all Kohn−Sham (KS) configurations. Energies were converged down to 10^{-6} Hartree and the largest norms during geometry optimization to 10^{-3} a.u.

The fully antiferromagnetic coupled electronic configurations were converged from higher M_S values using various spin down-coupling approaches: These included immediate full coupling, or gradual decreasing the M_S quantum number in steps of 1, or in difficult cases starting from an one-electron oxidized electronic guess wave function. These configurations in general exhibited a substantial amount of spin delocalization into ligand atoms, as is usually seen for high-spin systems.[43]

Cosmo Energies. To shield the electrostatic interactions within the protein, the conductor-like screening model (Cosmo)[48,49] was used with a dielectric constant of 10.[50] The optimized Cosmo radii in Turbomole were applied (H: 1.30 Å, C: 2.00 Å, N: 1.83 Å, O: 1.72 Å).[51] The radius for iron was set to 2.0 Å. It is known that Cosmo energies are very insensitive to the metal radius (but *not* to the other radii), since the metal is buried in complexes and thus not in contact with the probe.[52]

Model Systems. All structures were generated from the crystal structure of the diferrous wild type protein (pdb-code 1PIY). The chemical model included the beta carbons of the six first-sphere amino acids, and fixed parts of the second-sphere residues seen to interact via hydrogen bonds to these amino acids. The latter included Asp-237 modeled as formate, which interacts with His-118; the backbone of Gln-43 modeled as formamide, which interacts with His-241; NE1 of Trp-111, modeled as ammonia, which interacts with Glu-238 and Glu-204; the hydroxyl groups of Tyr-122 and Ser-114, modeled as water, interacting with Asp-84 and His-241, respectively; and the amine group of Gln-87, modeled as ammonia, interacting with Glu-204. Alpha carbons were changed into hydrogens to make methyl end groups, and fixed at the crystal structure positions to mimic the constraints of the scaffold, while still allowing flexibility within the site. O_2 and water were then bound to this 89-atom model, to build the candidate intermediates, with full geometry optimization of the antiferromagnetic coupled ground states and subsequent computation of the electrostatic screening effects. The hydrogens substituting alpha carbons in the 6 coordinating amino acids were frozen at the PDB coordinate (6 atoms), together with the Asp-237 formate model (4 atoms), the Gln-43 formamide model (6 atoms), and the heteroatoms and hydrogens resembling the nearest carbon in Tyr-122 (2 atoms) Ser-114 (2 atoms), Gln-87 (2 atoms), and Trp-111 (3 atoms). Altogether, 25 atoms were frozen at the PDB coordinates. Intermediate P is generally accepted as a cis μ-1,2 peroxide bridged diferric cluster, based on resonance Raman[21] and Mossbauer data.[26,28] Theoretically, other modes of peroxide coordination to a diferric site are feasible: trans μ-1,2 μ-1,1, μ-η^2,η^1 and μ-η^2,η^2, though these do not agree with experimental data. Regardless, we generated computer models for each of these potential intermediates and evaluated the energetics and spectroscopic properties in this study. The series of "**0**" intermediates (*vide infra*) were systematically generated using Arguslab, by changing the coordination mode of carboxylic residues and then performing partial relaxation of the ligand by force field methods without changing the remaining structure, to provide consistent and reasonable starting structures for all eight possibilities of open (i.e., nonbridged) and closed (i.e., bridged) Glu-238 coordination modes and syn and anti terminal carboxylate conformations. The "**w**" and "**h**" intermediates were made from respective optimized **0**-intermediates by adding water (**w**) and allowing dissociation into hydroxide + proton (**h**). In the protein structure, the water access channel leads to Fe1[10] and ENDOR results show that no protonated ligands are present on Fe2 in intermediate X.[53] Thus, water was added to Fe1 and studied systematically. The "**p**" structures were generated by addition of a proton to **01** and **01(5,5)** (*vide infra*), manually changing the carboxylate conformations, and subsequently optimizing the geometries.

Mössbauer Isomer Shifts. For computation of isomer shifts, we used a test set of nine iron complexes that displayed experimental isomer shifts well separated in the range from −0.18 to +0.61 mm/s and were of a reasonable size to handle computationally. These complexes have also been used as parts of larger calibration sets by Noodleman[54] and Oldfield.[55] Isomer shifts for candidate intermediates were obtained from calculating total electron density (sum of α and β density) on the iron atoms, and subsequently using a linear relation obtained from a same-method fit to experimental isomer shifts of the nine model complexes. Details of the fitting procedure are given in the Supporting Information, Table S1 and Figure S1. The full models were used for computation of isomer shifts.

Frequencies, Free Energies, and Excited States. Harmonic frequencies were computed to account for free energies of reaction and to correlate resonance Raman spectroscopic data with candidate intermediates. All computed frequencies were scaled by 0.98 which is a commonly applied scale factor for BP86/DZP type calculations.[56] As a test, some frequency calculations were carried out on the full models, representing typical structures (**03**, **09**, **012**, **w3**, and **h10**, *vide infra*) whereas frequencies were also computed for all structures with only first-sphere residues modeled as imidazole and acetate, to save computer time. The small-model Fe−O and O−O frequencies were accurate in all cases (see italic numbers in Table 2 for test calculations with the full models) and are presented throughout.

Zero-point energies and thermodynamic corrections were computed from the smaller models in order to estimate relative free energies. As the entropy of dissociating O_2 and water is almost constant among the models, the free energy corrections become similar in all complexes, and correction factors of 15.4 ± 1.9 kcal/mol for the nonhydrated models and 27.6 ± 1.1 kcal/mol for the hydrated models have been used. The free energies are presented relative to the computed deoxy state, which is in good agreement with the experimental structure (see Supporting Information, Figure S2), O_2, and in the case of hydrated models, water. However, the electronic energies (and the electronic component of the free energies) were computed from the large models, as these are sensitive to the geometry of second-sphere residues. The geometric details (equilibrium bond lengths) are shown in Table S2 (Supporting Information).

Time-dependent DFT (TDDFT) was used to compute the absorption spectra. The calculations were restricted to 150 excitations, which are enough to cover the region up to ca. 35 000 cm^{-1}, that is, within the UV−vis regime of the experimentally observed peroxo intermediates. Excitation energies were analyzed with the

(47) Weigend, F.; Ahlrichs, R. *Phys. Chem. Chem. Phys.* **2005**, *7*, 3297–3305.
(48) Klamt, A.; Schüürmann, J. *J. Chem. Soc., Perkin Trans.* **1993**, *2*, 799–805.
(49) Schäfer, A.; Klamt, A.; Sattel, D.; Lohrenz, J. C. W.; Eckert, F. *Phys. Chem. Chem. Phys.* **2000**, *2*, 2187–2193.
(50) Honig, B.; Nicholls, A. *Science* **1995**, *268*, 1144–1149.
(51) Klamt, A.; Jonas, V.; Bürger, T.; Lohrenz, J. C. W. *J. Phys. Chem. A* **1998**, *102*, 5074–5085.
(52) Jensen, K. P. *J. Inorg. Biochem.* **2008**, *102*, 87–100.
(53) Shanmugam, M.; Doan, P. E.; Lees, N. S.; Stubbe, J.; Hoffman, B. M. *J. Am. Chem. Soc.* **2009**, *131*, 3370–3376.
(54) Han, W.-G.; Liu, T.; Lovell, T.; Noodleman, L. *J. Comput. Chem.* **2006**, *27*, 1292–1306.
(55) Zhang, Y.; Mao, J.; Oldfield, E. *J. Am. Chem. Soc.* **2002**, *124*, 7829–7839.
(56) Scott, A. P.; Radom, L. *J. Phys. Chem.* **1996**, *100*, 16502–16513.

Table 2. Computed Properties of Peroxo-type Intermediates

name	ΔE^a/kcalmol^{-1}	ΔG^b/kcalmol^{-1}	Fe−O^c/cm^{-1}	O−O^d/cm^{-1}	J^e/cm^{-1}	EA^f/kcalmol^{-1}	$\delta-1$, $\delta-2^g$/mms^{-1}	λ^h/10^{3}cm^{-1}	comments^i
				Computed models without water					
01	**−34.9**	**−19.5**	447	957	−63	64.9	0.66	26 (23, 17, 12)	Closed
μ-1,2							0.66		syn-syn (6−5)
01(5,5)	**−35.1**	**−19.7**	416	1047	−16	70.9	0.58	20, 24 (15, 30)	Closed
μ-1,2							0.57		syn-syn (5−5)
02	−18.1	−2.7	413	1076	−63	70.2	0.41	28 (21, 17, 11)	Closed
μ-1,2							0.54		syn-anti (5−5)
03	**−28.0**	**−10.7**	*390*^{j}	*1037*	−352	69.4	0.61	28 (24, 20, 13)	Closed
μ-1,2			387	1030			0.61		anti-anti (5−5)
04	**−26.3**	**−10.9**	481	832	−33	68.8	0.67	24 (17, 13)	Closed
μ-1,2							0.68		anti-syn (5−6)
05	−15.6	−0.2	516	775	−177	71.8	0.49	28 (20, 13)	Open
μ-1,2							0.49		syn-syn (5−6)
06	**−32.3**	**−16.9**	467	1034	−318	58.9	0.63	28 (25, 15)	Open
μ-1,2							0.63		syn-anti (6−6)
07	**−25.6**	**−10.2**	406	1014	−83	71.7	0.52	27 (20, 14)	Open
μ-1,2							0.50		anti-anti (4−6)
08	**−28.9**	**−13.5**	404	1079	−408	67.4	0.68	27 (14)	Open
μ-1,2							0.69		anti-syn (5−6)
09	−15.0	−1.5	*397*	*1075*	−97	67.9	0.66	29 (21, 10)	Closed
μ-1,1			392	1064			0.66		syn-syn (6−5)
010	−15.9	−0.5	493	875	−106	72.3	0.65	25 (12)	Open
μ-η^2,η^2							0.67		syn-syn (5−6)
011	−12.5	2.9	438	837	−84	72.1	0.54	26 (17, 10)	Open
μ-η^2,η^2							0.53		anti-anti (4−5)
012	−11.8	3.6	*428*	*893*	−104	68.9	0.50	26 (20, 14)	Open
μ-η^2,η^1			439	896			0.51		syn-anti (5−5)
013	−20.3	−4.9	408	1051	−181	69.3	0.54	24 (18, 14)	Bidentate Fe2
μ-1,2							0.58		syn-anti (5−6)
				Computed water adducts: water bound in H_2O form					
w1	**−31.5**	**−3.9**	435	930	−266	65.2	0.70	26 (20, 14, 10)	Closed $H_2O(1)$
μ-1,2		**(15.6)**					0.70		syn-syn (6−6)
w2	**−31.5**	**−3.9**	453	842	−184	74.0	0.51	27 (20, 12)	Open $H_2O(1)$
μ-1,2		**(−1.2)**					0.47		syn-anti (5−5)
w3	−25.9	0.6	*412*	*937*	−235	63.0	0.55	25 (19, 12)	Open $H_2O(1)$
μ-η^2,η^1		(11.3)	404	940			0.57		anti-anti (5−5)
w4	**−37.6**	**−10.0**	437	1038	−266	68.2	0.57	27 (23, 14)	Open $H_2O(1)$
μ-1,2		**(0.9)**					0.56		anti-syn (5−5)
w10	−24.4	3.2	455	806	17	61.0	0.67	27 (23, 12)	Open $H_2O(1)$
μ-η^2,η^2		(3.7)					0.66		syn-anti (5−5)
wFe2	**−40.1**	**−12.5**	406	1054	−506	64.2	0.65	27 (24, 14)	Open $H_2O(2)$
μ-1,2		**(4.4)**					0.70		syn-anti (6−5)
				Computed water adducts: water bound in OH^- form with (partially) protonated O_2					
h1	**−26.2**	**1.4 (+5.3)**	411	851	11	65.7	0.56	28/25 (16)	Open OH(1)
μ-1,2		**(20.9)**					0.53		syn-syn (5−6)
h2	−19.3	8.3 (+12.2)	383	940	−208	65.5	0.55	29 (25, 19, 13)	Open OH(1)
μ-1,2		(11.0)					0.56		syn-syn (5−6)
h3	−20.0	7.6 (+7.0)	430445	913	−44	58.2	0.47	25 (16, 11)	Open OH(1)
μ-1,2		(18.3)					0.47		syn-anti (5−5)
h4	−21.9	5.7 (+15.7)	442	829	−154	65.2	0.46	27 (20, 8)	Open OH(1)
μ-1,2		(16.6)					0.51		syn-syn (5−5)
h10	−12.9	14.7	*409*	*823*	−18	71.6	0.56	23 (17, 9)	Open OH(1)
μ-η^2,η^2		(+14.1)	426	829			0.60		syn-anti (5−5)
		(15.2)							
				Protonated: exogenous proton added to non-hydrated complexes and reoptimized^k					
p1Acs	−65.4	−50.0	785	no O_2 bond	361	116.1	0.33	5, 13, 19, 23	Closed O−H−O
Broken		(−30.5)					0.37		syn-syn (6−5)
p1Bcs	−65.7	−50.3	702	no O_2 bond	643	108.2	0.36	6, 13, 20, 23	Closed O−H−O
Broken		(−30.8)					0.32		syn-syn (6−5)
p1*Acs	−60.8	−45.4	500	724	−47	100.3	0.52	8, 13, 21, 28	Closed AspH
μ-1,2		(−25.9)					0.52		syn-syn (5−5)
p1*Bcs	−64.1	−48.7	707	no O_2 bond	613	88.7	0.25	5, 13,23	Closed O−H−O
Broken		(−29.2)					0.28		syn-syn (5−5)
p1*Aos	−59.3	−43.9	376	964	−10	100.7	0.59	8, 15, 21, 27	Closed AspH
μ-1,2		(−24.4)					0.59		syn-syn (5−6)
p1*Bos	−42.0	−26.6	353	772	59	109.1	0.51	6, 15, 20, 29	Open μ-GluH
μ-1,2		(−7.1)					0.56		syn-syn (5−5)
p1*Ao′s	−61.4	−46.0	489	727	110	101.0	0.55	8, 13, 21, 28	Closed AspH
μ-1,2		(−26.5)					0.55		syn-syn (5−5)
p1*Bo′s	−59.0	−43.6	459	815	170	100.4	0.54	7, 11, 16, 21, 30	Open GluH-μGlu
μ-1,2		(−24.1)					0.53		syn-syn (5−5)

Table 2. Continued

name	ΔE^a/kcalmol^{-1}	ΔG^b/kcalmol^{-1}	Fe−O^c/cm^{-1}	O−O^d/cm^{-1}	J^e/cm^{-1}	EA^f/kcalmol^{-1}	$\delta-1$, $\delta-2^g$/mms^{-1}	λ^h/10^{3}cm^{-1}	comments^i
p1*Aca′	−58.7	−43.3	384	945	12	101.2	0.58	5, 10, 16, 23, 28	Closed AspH
μ-1,2		(−23.8)					0.58		syn-anti (5−5)
p1*Bca′	−61.8	−46.4	521	809	−98	97.7	0.58	8, 13, 20, 25, 30	Closed GluH
μ-1,2		(−26.9)					0.58		syn-anti (6−5)
p1*Aoa	−58.8	−43.4	385	950	9	100.9	0.58	5, 16, 23, 28	Closed AspH
μ-1,2		(−23.9)					0.58		syn-anti (5−5)
p1*Boa	−66.6	−51.2	401	1054	13	82.3	0.58	8, 20, 30	Open GluH-μGlu
μ-1,2		(−31.7)					0.57		syn-syn (5−6)
p1*Aca	−61.5	−46.1	468	724	−42	98.8	0.55	8, 13, 18, 21, 28	Closed AspH
μ-1,2		(−26.6)					0.54		syn-syn (5−5)
p1*Bca	−68.5	−53.1	494	779	374	112.4	0.60	8, 14, 21, 26, 0	Closed GluH
μ-1,2		(−33.6)							syn-syn (6−5)

[a] Computed electronic energy with electrostatic screening of $\varepsilon = 10$ from Cosmo. [b] Computed free energy from electronic energy, frequencies, and standard thermodynamic analysis; $\Delta\Delta G$ values for hydration are given in parentheses for the w-models and h-models (last parentheses). For h-models, first parentheses shows free energy change from corresponding w model. For p models, the parentheses shows free energy of binding a proton to **01** to form the relevant complex. [c] Fe−O stretch frequency. [d] O−O stretch frequency. [e] *J*-coupling constant between Fe1 and Fe2. [f] Electron affinity computed from difference in electronic energies of fully relaxed reduced and oxidized geometries. [g] Mössbauer isomer shifts of Fe1 and Fe2. [h] Computed maxima in the absorption profile (and other peaks in parentheses) in units of 1000 cm^{-1}. [i] Numbers in parentheses refer to coordination number of Fe1−Fe2. [j] The underlined italic numbers were computed from the full models, the regular-style numbers with the small model. [k] The **p1** and **p1*** models were derived from **01** and **01(5,5)**, respectively; A and B denote the proton was added to the O closest to Fe1 and Fe2, respectively; "o" and "c" refer to open and closed conformation of Glu-238; "a" and "s" refer to anti and syn conformations of Glu-204; and the prime denotes that this perturbation was performed subsequent to proton addition.

software Swizard,[57] and absorption profiles were simulated from Gaussian fitting with an average line width of 3000 cm^{-1}, using superposition of elementary transitions from the TDDFT calculations. For calibration, TDDFT calculations were performed on a model of the oxo bridged biferric state and with the addition of a proton to the bridge. The spectral change reasonably reproduced the oxo to Fe(III) CT transitions of the met state (see Supporting Information).

J-coupling constants were computed from the Heisenberg spin Hamiltonian $\hat{H} = -JS_1 \cdot S_2$ rearranged into Equation 1,[58] assuming ferric sites in P and P′ and using $S_1 = S_2 = 5/2$ in the true antiferromagnetic state (see reference[58] for details):

$$J \approx \frac{-(E_{M_S=S_{max}} - E_{M_S=0})}{2S_1S_2} = \frac{-(E_{M_S=S_{max}} - E_{M_S=0})}{2 \cdot \left(\frac{5}{2} \cdot \frac{5}{2}\right)} = \frac{-2(E_{M_S=S_{max}} - E_{M_S=0})}{25} \quad (1)$$

In this equation, $E_{M_S=5}$ is the energy of the electronic configuration of the complex with 10 excess alpha (spin-up) electrons and $E_{M_S=0}$ is the energy of the fully antiferromagnetically coupled broken-symmetry configuration.

Results and Analysis

Computed Properties of Possible Peroxo-Like Intermediates. Table 2 displays a variety of computed properties of structurally distinct, *a priori* possible peroxo-type intermediates, from successfully converged and geometry optimized calculations. The corresponding structures are shown in Figure 3. Models beginning with "**0**" do not have a water molecule bound, models beginning with a "**w**" have a water bound to iron, those beginning with an "**h**" have a water bound in the form of a hydroxide and a proton, and those with a "**p**" have a proton added to the **01** and **01(5,5)** structures (*vide infra*).

Table 2 shows the computed properties listed in the order of relative electronic energies, relative free energies, Fe−O and O−O stretching frequencies, *J*-coupling constants, electron affinities, isomer shifts, and maxima in the absorption profiles computed from TDDFT. Isomer shifts are listed as Fe1 first, then Fe2 (Fe1 is bound by Asp-84 and Fe2 by Glu-204, Figure 1). To aid in the structural differences between these structures, comments have been added in the final column of Table 2: *Closed* and *open* refers to whether Glu-238 is bridging both irons or only binding directly to Fe2, respectively. When water is bound (second part of Table 2), a number in parentheses indicates whether water is bound to Fe1 or Fe2. *Anti-* and *syn-*conformations of Asp-84 and Glu-204, respectively, are also designated, and finally the coordination numbers of Fe1−Fe2 are given in parentheses.

While O_2-binding energies are sensitive to hydrogen bonds and surrounding effects, the O−O and Fe−O stretching frequencies are not, as can be seen from comparing frequencies obtained with both models in the fourth and fifth columns of Table 2. Differences in Fe−O and O−O stretch frequencies were generally smaller than 10 cm^{-1} in the large (italic, underlined) and small models.

It became clear early in the computational efforts that structures with a μ-1,2 coordination geometry of O_2 are by far the most stable, so this coordination mode has been studied systematically. The free energies of species that are considered thermodynamically accessible within the uncertainties of the method have been written in bold. The distinction between cis- and trans-μ-1,2 isomers can be deduced by inspection of Figure 3.

Nonhydrated Models: Free Energies and O−O Stretch Frequencies. The first section of Table 2 contains models without a water molecule bound. As shown in Figure 3, **01**−**08** designate μ-1,2 type intermediates, with **01**−**04** having closed structures and **05**−**08** having open structures; the models 1/5 have syn-syn conformations of the terminal carboxylates; 2/6 are syn-anti; 3/7 are anti-anti; and 4/8 are anti-syn. Representative structures of other coordination geometries are models **09** to **013**. In model **09**, O_2 is bound in a μ-1,1 fashion; **010** and **011** are syn-syn and anti-anti structures of the μ-η^2,η^2 geometry; and **012** is in a twisted conformation where two oxygens bind Fe1 and only one oxygen bind Fe2 (μ-η^2,η^1). An additional,

(57) Gorelsky, S. I. Swizard Program, revision 4.4, 2008, http://www.sg-chem.net/.
(58) Noodleman, L.; Han, W.-G. *J. Biol. Inorg. Chem.* **2006**, *11*, 674–694.

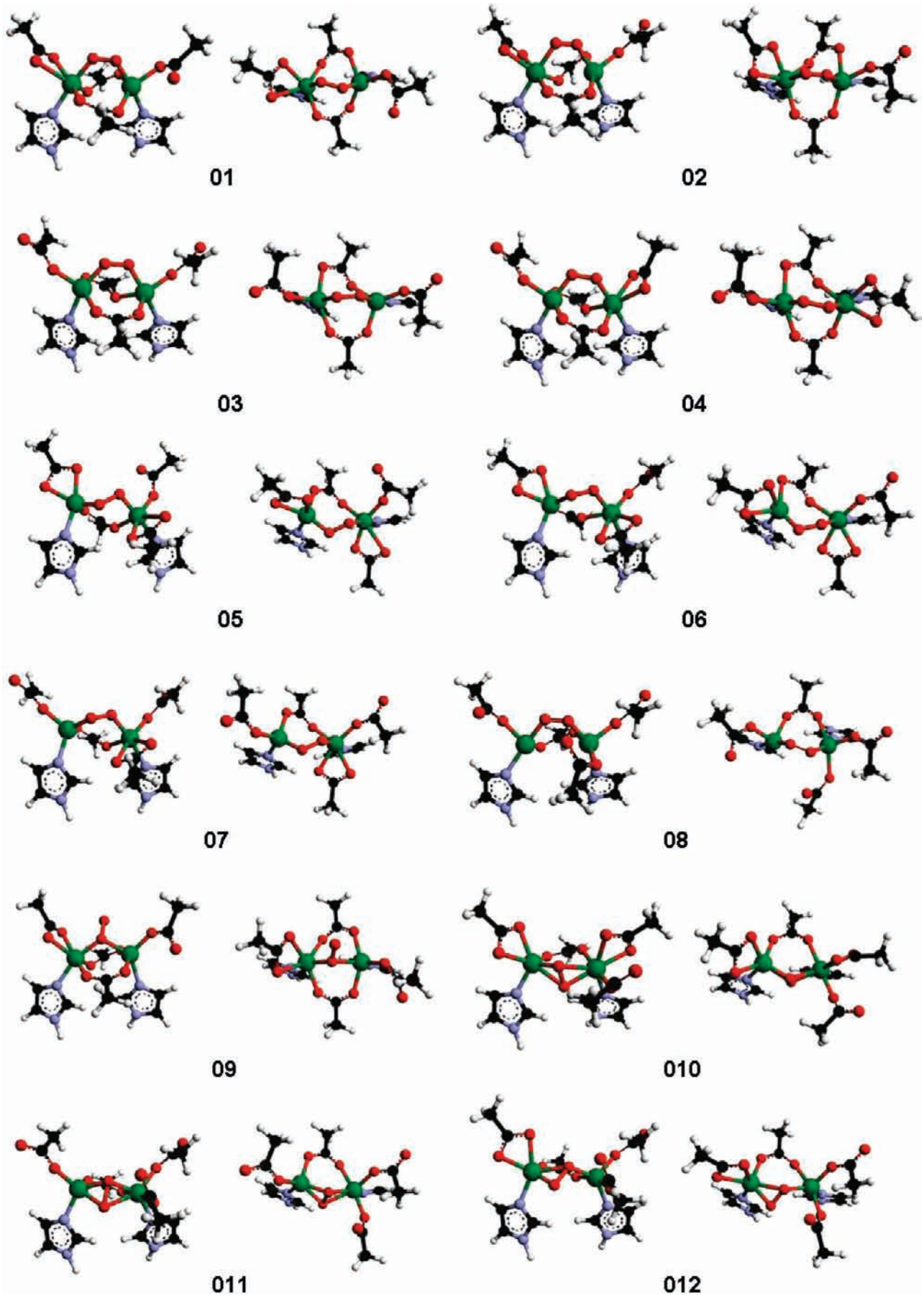

Figure 3. Continued.

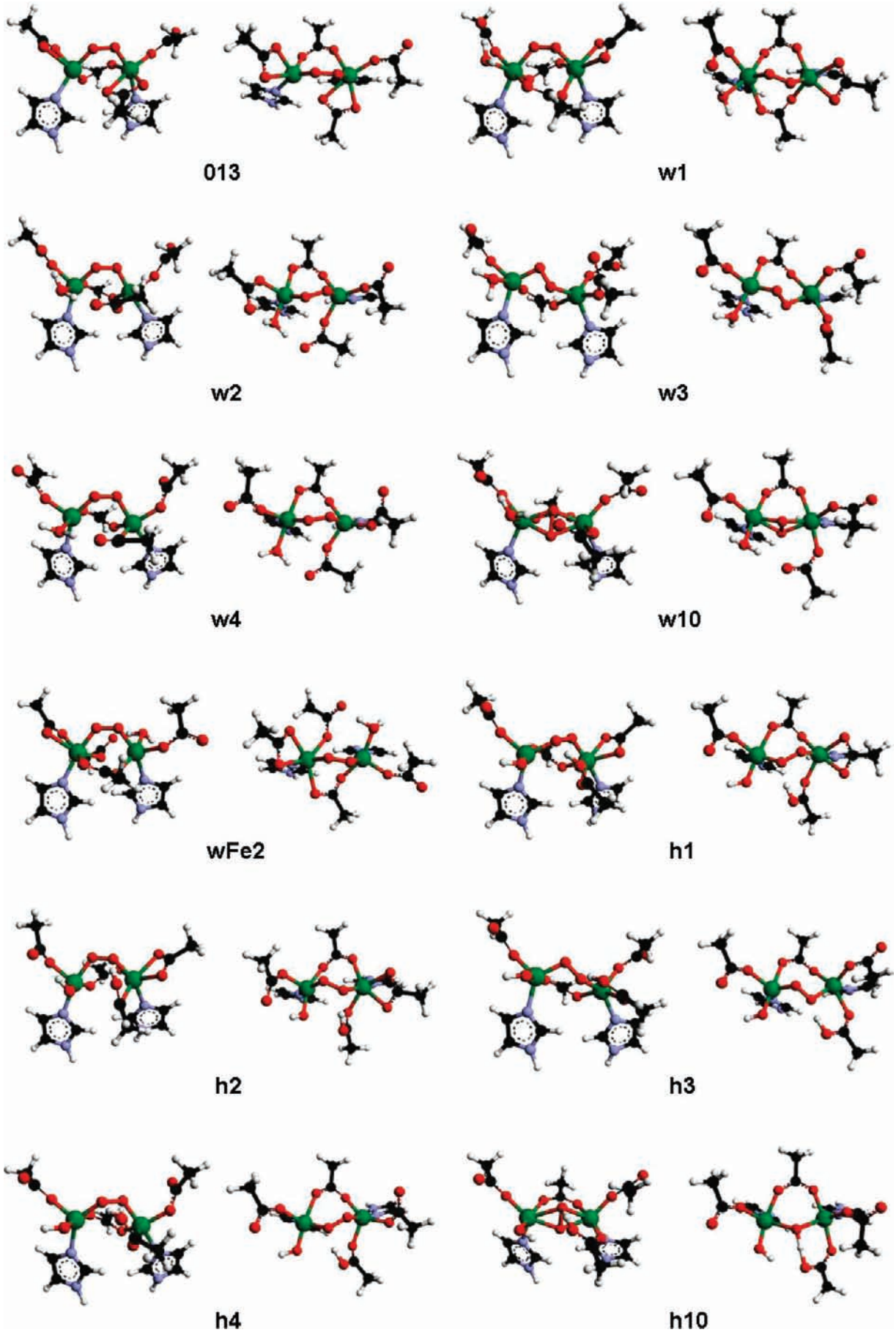

Figure 3. Continued.

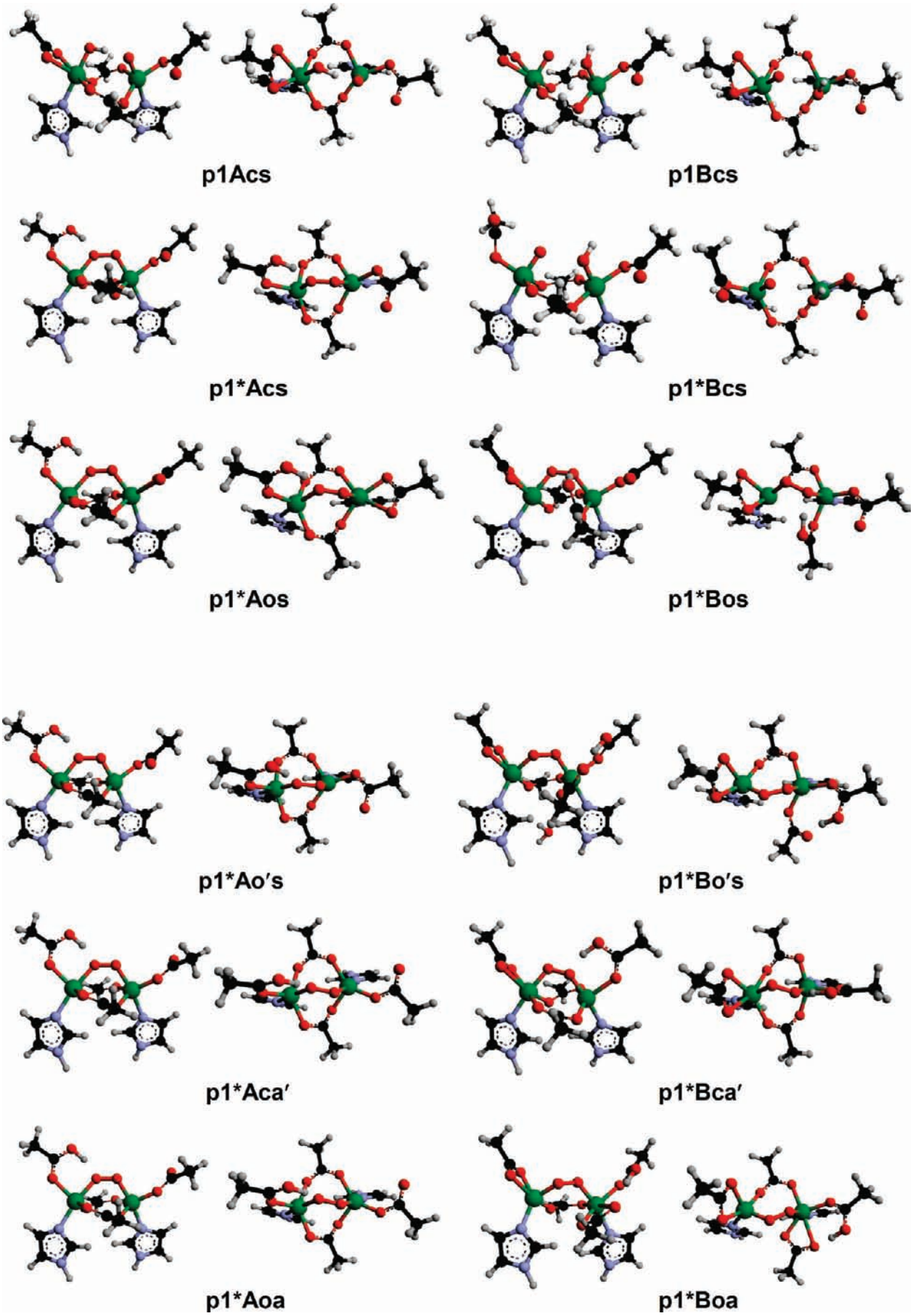

Figure 3. Continued.

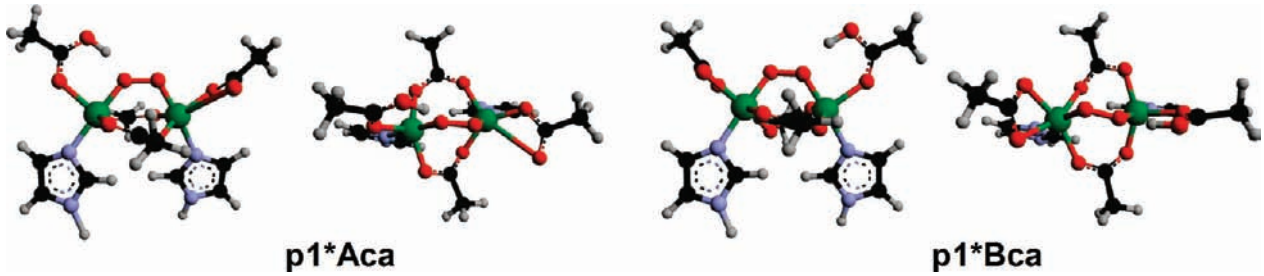

Figure 3. (Continued) Equilibrium structures of geometry-optimized models. Fe1 is left and Fe2 is right.

unusual structure (**013**) was found with Glu-238 bound bidentate to Fe2 instead of bridging the irons (the Fe1−O distance is 2.63 Å in this structure).

Free Energies. The free energies correspond to the reaction of O_2 binding to the uniquely determined deoxy state, which is in agreement with the experimental structure (see Supporting Information), to form the peroxo intermediate. To focus on possible biologically relevant structures, we used an estimate of the uncertainty in free energies of isomers of 5 kcal/mol, which is a conservative estimate considering that μ-1,2 type isomers are isodesmic and that such an accuracy of DFT has been estimated for other nonisodesmic reactions.[59] Furthermore, a thermodynamic "buffer" of 5 kcal/mol was included, so that any complex having a free energy within 10 kcal/mol of the most stable candidate was included. With these selection criteria, **01**, **03**, **04**, **06**, **07**, and **08** represent thermodynamically accessible candidates within the uncertainty of the computational method. Furthermore, these structures are all at least an additional 5 kcal/mol more stable than the remaining structures, implying that the selection is strict.

The most stable of these six structures is **01** (−19.5 kcal/mol for the computed free energy of binding O_2 to the deoxy state), in which the two terminal carboxylates are in syn conformations, and Glu-238 is still bridging. Thus, this structure, in addition to being the most stable, also represents the smallest structural reorganization upon O_2 binding to the known deoxy structure. The coordination numbers 6 and 5 for Fe1 and Fe2 reflect that the carboxylate on Fe1 has gone bidentate and Glu-204 monodentate upon O_2-binding.

Importantly, the representative alternative coordination modes of O_2 are all at least 9 kcal/mol less stable than the least stable of the above-mentioned models, and the most stable of them, the μ-1,1 coordination mode in **09** (−1.5 kcal/mol), is 18 kcal/mol less stable than the structure with the lowest free energy, **01** ($\Delta G = -19.5$ kcal/mol). *Thus, all energetically accessible intermediates display μ-1,2 type coordination modes.* On the basis of these results, we concentrate on the μ-1,2 type structures. We also found a stable equilibrium geometry for the **01** structure with coordination numbers of 5 and 5, with a ΔE of −35.1 kcal/mol, that is, isoenergetic with **01** with coordination numbers 6 and 5, showing that both are energetically accessible (see Table 2).

Vibration Frequencies. The peroxo intermediate experimentally observed in the W48F/D84E double mutant of RNR has $\nu_{Fe-O} = 457$ cm^{-1} and $\nu_{O-O} = 868$ cm^{-1}.[29] A viable calculated peroxo intermediate is expected to display similar values.

The computed Fe−O and O−O stretch frequencies are shown in the fourth and fifth columns of Table 2. In case of pseudosymmetric models (e.g., μ-1,1; μ-1,2; and μ-η^2,η^2) only the symmetric Fe−O stretches have been included in Table 2. For asymmetric models (μ-η^2,η^1) the modes most resembling symmetric Fe−O stretches were included. Importantly, for the O−O stretch there is never any ambiguity. Among the energetically viable candidates mentioned above, those with O−O stretch frequencies close to 800−900 cm^{-1} are peroxo species with a weakened O−O bond due to additional electron donation into the O_2 π^* orbital from the irons. Among the six possible structures, **01** has $\nu_{Fe-O} = 447$ cm^{-1} and $\nu_{O-O} = 957$ cm^{-1}, and **04** has $\nu_{Fe-O} = 481$ cm^{-1} and $\nu_{O-O} = 832$ cm^{-1}, while **03**, **06**, **07**, and **08** all have ν_{O-O} above 1000 cm^{-1}. Model **01** is substantially more stable than **04**, and other computed properties of **01** are also consistent with the peroxo intermediate (*vide infra*). Note that for **01(5,5)** in Table 2, ν_{O-O} is at 1047 cm^{-1} and ν_{Fe-O} is at 416 cm^{-1} indicating that less charge has been transferred from the deoxy site to O_2 upon binding. However, this species has five β and five α unoccupied orbitals having dominantly Fe character, indicating that it is still best described as a μ-1,2 peroxy bridged diferric species.

An important result so far is the observation that specific changes in the carboxylate conformations can substantially tune the electronic structure of the O−O bond. This is seen in the decrease in isomer shifts and increased ν_{O-O} upon opening of the bridging carboxylates or upon terminal carboxylates going syn to anti, both reflecting less electron donation to O_2.

Hydrated (H_2O) Models: Free Energies and O−O Stretch Frequencies. The second section of Table 2 summarizes the results for models where an additional water has been bound to the site after O_2 binding. These were generated by addition of a water molecule to Fe1 of the four closed models, including the two possible P intermediates **01** and **04**, and the structures were geometry optimized. Since the crystal structure of the deoxy state and the computed structures for the best peroxo candidates (**01, 01(5,5)** and **04**) are closed, water binding to already open structures was not considered.

The structure **w10** provides an example of water binding to a model with a μ-η^2,η^2 coordination geometry, showing that water binding is feasible in such structures as well. The free energy of this structure, +3.2 kcal/mol, representing both O_2 and water-binding to the deoxy state, is not energetically competitive with the μ-1,2 structures. However, it is considerably more competitive in the hydrated models than in the nonhydrated models, and this may be one explanation why a μ-η^2,η^2 peroxo intermediate has been found in calculations of MMO, where a water is bound in the models.[60]

Model **wFe2** illustrates that, in principle, water binding to Fe2 is thermodynamically feasible, if a coordination site and water access were available. Such binding would likely open

(59) Siegbahn, P. E. M. *J. Biol. Inorg. Chem.* **2006**, *11*, 695–701.

(60) Rinaldo, D.; Philipp, D. M.; Lippard, S. J.; Friesner, R. A. *J. Am. Chem. Soc.* **2007**, *129*, 3135–3147.

the bridging carboxylate from Fe2 instead of on Fe1 (*vide infra*). In the final met structure (Figure 1) Glu-238 is opened from Fe1.

From the water adduct structures (**w1**−**w4**) in Figure 3, except for **w1,** geometry optimization after addition of the water caused the initially closed structure to open. *Thus, it is a result from this study that water most often acts as a substitution reagent, displacing the bridging carboxylate from the water-bound iron, resulting in the open structure observed in the met crystal structure.* In all structures, except **w1**, such behavior is observed, reflecting the steric and electronic restrictions of having both a carboxylate and water binding to iron at the same coordination site. In **w1**, the syn conformation of Asp-84 stabilizes the additional ligand by hydrogen bonding, while the syn conformation of Glu-204 makes it less favorable to open the structure. An interesting point here is the difference between the WT and the D84E mutant of RNR. In the protein structures, the water channel leads directly to Asp-84. In the WT, Fe1 is likely 5-coordinate in the μ-1,2-bridging peroxo structure, so an open coordination position is available for water binding, and water could provide a proton to activate the O−O bond.[29] In the D84E mutant, Fe1 would be 6-coordinate in P, preventing water from binding, and thus trapping this peroxo species as experimentally observed.[12]

Free Energies. The computed electronic energies and free energies of binding both water and O_2 to the deoxy model are shown in Table 2 for each resulting adduct. The most stable form of the four relevant water adducts is **w4** (−10.0 kcal/mol). Two other structures, **w1** and **w2**, have free energies that are within 10 kcal/mol of **w4**. Thus these are mechanistically possible models with negative free energies of binding both water and dioxygen. Since these energies are absolute binding energies, they have larger uncertainties than 5 kcal/mol associated with them, but the relative stability of the isomers should still be accurate to within ca. 5 kcal/mol (Table S4 in Supporting Information). On the other hand, we estimate the uncertainty in the absolute binding free energy to be at least 10 kcal/mol, as bond dissociation energies are sensitive to factors such as the amount of exact exchange in the functional.[45]

Using the corresponding nonhydrated O_2 adduct as the reference, the free energy of hydration of each intermediate is computed to be +15.6 kcal/mol for **01**, −1.2 kcal/mol for **02**, +11.3 kcal/mol for **03**, and +0.9 kcal/mol for **04**. These free energies of hydration span a significant range and depend critically on the molecular structures of the individual sites. For example, binding water to **01** requires a large reorganization at Fe1 and makes the hydrated structure relatively unfavorable, in comparison to the other, open, structures where less steric strain is encountered upon hydration. Water binding to the anti-anti structure **03** is unfavorable because Asp-84 changes conformation to bind to water and the resulting water adduct is very open giving rise to an unusual geometry with O_2 in a slightly twisted coordination mode. In **02** and **04** on the other hand, structural changes upon water binding are minor, and the energy of binding is favorable.

Vibration Frequencies. We can again assess the nature of the O−O bond in the water adducts. As mentioned above, Raman data were recorded on the W48F/D84E double mutant. MCD results show that Glu-84 is bidentate in the deoxy state of this mutant, whereas in the WT, Asp-84 is monodentate.[11] An added water molecule would then be able to bind to Fe1 in the WT peroxy structure, taking up the sixth coordination site.

From Table 2, several of the hydrated models have O−O stretch frequencies that are in the range observed for P making a water-bound peroxo intermediate a viable possibility. Of the energetically and mechanistically feasible structures, both **w1** and **w2** have peroxo-like electronic structures as judged from the computed frequencies: **w1** has $\nu_{Fe-O} = 435$ cm^{-1} and $\nu_{O-O} = 930$ cm^{-1}, whereas **w2** has $\nu_{Fe-O} = 453$ cm^{-1} and $\nu_{O-O} = 842$ cm^{-1}, both consistent with P.

Hydrated (OH^- + H^+) Structures: Free Energies and O−O Stretch Frequencies. In the next section of Table 2, we have evaluated the possibility of having the water bound dissociatively to give hydroxide on Fe1 and a proton. Partial protonation of O_2 could activate the O−O bond by increasing electrophilicity (i.e., stabilizing the Fe(III)-O_2^{2-}-Fe(III) resonance form via the positive charge on the proton). Therefore, we also computed hydroxide counterparts to the five models **w1**−**w4** and **w10**. These structures were generated by moving the water proton closest to O_2 to the nearest oxygen atom (O_A) and then geometry optimizing the structures. The corresponding geometry optimized structures are designated **h1**−**h4** and **h10** and are shown in Figure 3. The corresponding computed properties are shown in the third section of Table 2.

Free Energies. It was possible to find stable minima for all five structures with a bound hydroxide. In all cases, the proton resides on Glu-238 and H-bonding to the O_2. Furthermore, in all cases, the structure is open: the initially closed **w1** structure opens when Glu-238 becomes partially protonated and loses its ability to coordinate iron.

As the hydroxide structures are isomers of the water models, the free energies can be compared directly between the two groups of structures. The structure **h1** represents the most stable hydroxide isomer, with a free energy of +1.4 kcal/mol. This energy is reasonably competitive with the free energies of **w1** and **w2**, implying that deprotonation of the coordinated H_2O is uphill by 5.3 kcal/mol. However, the other hydroxide structures seem too unstable to be relevant.

All comparable models where a proton has moved from H_2O to between Glu-238 and O_2 are less favorable by at least 5 kcal/mol. Model **h1** has the hydrogen bond from Fe1 bound hydroxide to Tyr-122 and from Tyr-122 to the dangling oxygen of Asp-84, whereas in **h2** the hydrogen bond is directly from the bound hydroxide to the dangling oxygen of Asp-84. In **h1**, O_A is partially protonated as expected, whereas in **h2**, the proton is H-bonding to O_B. The **h1** structure is 6.9 kcal/mol more stable than **h2**. In **h1**, the proton is located on Glu-238, with a 1.07-Å O−H distance, with a very strong hydrogen bond to O_2; the H−O distance is only 1.46 Å.

Vibration Frequencies. When O_2 is partially protonated, all O−O stretch frequencies now fall into the region of $\lesssim$1000 cm^{-1}. This observation implies increased stabilization of the electron density on the peroxide due to electrostatic polarization by the proton. The relatively stable structure **h1** has $\nu_{O-O} = 851$ cm^{-1} and $\nu_{Fe-O} = 411$ cm^{-1}, typical of a peroxo-type intermediate. Hence, it is feasible to have peroxo-type intermediates with partial protonation or a very strong hydrogen bond (an O−H distance of 1.46 Å); such a **h**-structure will necessarily be open and also tend to have a syn conformation of Asp-84. In fact, all "**h**" species in Table 2 optimized to a syn conformation of Asp-84. This is due to loss of the bridging carboxylate leading to the increased ferric nature of Fe1 when OH^- is bound, as reflected in the lower isomer shifts (*vide infra*).

Proton only Models: Free Energies and O−O Stretch Frequencies. The last section of Table 2 contains models where a proton was added to both sides of the bound peroxide in **01** (**p1** structues) and **01(5,5)** (**p1*** structures). For **p** structures the "A" or "B" refers to the proton being placed on the oxygen bound to Fe1 or Fe2 (now referred to as O_A or O_B), respectively; models with an "o" or "c" refer to whether the initial structure was open or closed and "a" or "s" refer to anti and syn conformations of the terminal Glu-204 prior to geometry optimization. The prime after these letters denotes that this structural perturbation was performed subsequent to addition of the proton and optimization. As shown in Figure 3, the bridging and terminal carboxylates are varied in the resulting final structures. In all cases where the starting geometry was open and Asp-84 was protonated (all "Ao" models, in Table 2) the site closed during optimization. Model **p1*Bos** is the singular example of the proton bound to the previously bridging carboxylate. Structures with a bridging OOH moiety were not stable and resulted in OO bond cleavage and isomer shifts in the 0.25 to 0.37 mm/s range, **p1Acs**, **p01Bcs** and **p1*Bcs**. These models have interesting implications for the O_2 reaction in MMO, but are not analyzed further here.

Free Energies. The most stable structure is **p1*Bca** with a free energy of −53.1 kcal/mol. All other structures are within ∼10 kcal/mol except for **p1*Bos** which is 26.5 kcal/mol uphill. This shows that protonation of the bridging Glu is energetically unfavorable and does not represent a viable peroxo intermediate. Candidates **p1*Bo′s** and **p1*Boa** converged to interesting geometries where the H^+ is located between the two carboxylates bound to Fe2. These, however, would require a large reorganization energy and are not consistent with the fast kinetics of peroxo intermediate formation in WT. For all remaining viable models (**p1*Acs**, **p1*Aos**, **p1*Ao′s**, **p1*Aca′**, **p1*Bca′**, **p1*Aoa**, **p1*Aca** and **p1*Bca**) the structures are closed and the terminal carboxylate on either Fe1 or Fe2 is protonated and H-bonding with the peroxide. The free energy for adding a proton from solvent to the **01** and **01(5,5)** viable peroxy bridged P intermediates is −23.8 to −33.6 kcal/mol; therefore it is quite favorable to protonate a peroxy structure if the proton is available.

Vibration Frequencies. For all **p**-structures where the O−O bond did not cleave, the O−O stretching frequencies fall into two categories; 724 to 815 cm^{-1} and 945 to 1054 cm^{-1}. In all cases O_2 is partially protonated (i.e., H-bonded to the terminal carboxylate) and the frequency correlates directly with the O−O bond length (ranging from 1.41 Å in **p1*Acs**, **p1*Aca** and **p1*Ao′s** to 1.32 Å in **p1*Boa**). Models with higher O−O frequencies tend to have lower Fe−O frequencies and longer average Fe−O bond lengths. The H-bond to the peroxide resulted in elongation of the associated Fe−O bond and slight asymmetry and twist in the Fe−O_2−Fe unit toward the H-bond.

In summary, from a systematic search of potential peroxo-type structures within the RNR architecture, the energetically viable structures are **01**, **03**, **04**, **06**, **07**, **08**, **w1**, **w2**, **w4**, **h1**, **p1*Acs**, **p1*Aos**, **p1*Ao′s**, **p1*Aca′**, **p1*Bca′**, **p1*Aoa**, **p1*Aca** and **p1*Bca**. Among these, the nonhydrated models **01** and **04**, the hydrated models **w1** and **w2**, the hydrated deprotonated model **h1,** and the closed **p**-structures with protonated terminal carboxylates represent viable peroxo intermediates. We now consider other computed properties and evaluate how they relate to the optimized geometries of these structures.

Nonhydrated Models: *J*-Coupling Constants and Isomer Shifts. *J*-Coupling Constants. The *J*-coupling constants have rather large uncertainties associated with them due to the bias of different functionals toward the high-spin state of eq 1. Exact exchange will tend to lower the energy of the high-spin state and thus shift the exchange toward weaker antiferromagnetic coupling. We estimate a standard error of ∼50 cm^{-1} in these values, based on test calculations with the B3LYP functional. A value of −50 cm^{-1} was experimentally observed for P in the W48F/D84E double mutant of RNR.[35] Using this value as a rough guideline, we consider a computed *J*-coupling constant in the range −100 to +0 cm^{-1} as reasonable for a peroxo-type intermediate in RNR.

From Table 2 all nonhydrated models are found to be antiferromagnetically coupled. Most have couplings in the expected range, though **03** (−352 cm^{-1}), **06** (−318 cm^{-1}), and **08** (−408 cm^{-1}) are too strongly coupled. These three structures have higher O−O stretch frequencies, thus more charge donated from the peroxide to the Fe(III) ions.

The two candidates for stable peroxo intermediates in this group, **01** and **04**, have computed *J*-coupling constants of −63 cm^{-1} and −33 cm^{-1}, respectively, in the anticipated range. However, most other structures, including some with high O−O stretches (**02**, **07**, **09**) and some with alternative O_2 coordination geometries (**09**, **010**, **011**, **012**) fall in this group, so the extent of coupling between the iron sites is not in itself a sufficient (although necessary) requirement for correlating to peroxo intermediates.

Mössbauer Isomer Shifts. The computed isomer shifts have estimated uncertainties of less than 0.1 mm/s for absolute values and ∼0.03 mm/s for relative values, i.e. when comparing differences in isomer shifts between similar structures (see Table S5, Supporting Information). The computed values of the isomer shifts probe the electron density at the iron nuclei and provide information about the effective oxidation state of the irons.

A first observation from all of Table 2 is that the isomer shifts can be divided into three distinct groups; one with shifts from 0.61−0.68 mm/s, one with shifts from 0.49−0.58 mm/s and one with shifts less than 0.37 mm/s.[61] The latter corresponds to **p**-structures where the O−O bond has cleaved. The former two groups are an interesting result, since the observed intermediates P and P′ each fall into one of these groups.

Among the comparable μ-1,2 structures, the two peroxo intermediates, **01** and **04**, display isomer shifts of 0.66/0.66 mm/s and 0.67/0.68 mm/s, both in good agreement with experimental values of for P intermediates.[26,28] Three other structures have isomer shifts in the range expected, **03**, **06**, and **08,** but they have high ν_{O-O} frequencies inconsistent with that observed experimentally for P. The isomer shifts correlate with the amount of negatively charged carboxylate oxygen atoms close to iron. This can be seen by comparing the syn-to-anti conformational changes for each group of structures, that is, **01** → **02** (0.66/0.66 mm/s → 0.41/0.54 mm/s); **04** → **03** (0.67/0.68 mm/s → 0.61/0.61 mm/s); and **08** → **07** (0.68/0.69 mm/s → 0.52/0.50 mm/s). Upon going from **05** → **06** (0.49/0.49 mm/s → 0.63/0.63 mm/s) the opposite bridging carboxylate Glu-115 goes

(61) The only exception is **02**, which has an unusual difference in isomer shifts of Fe1 (0.41 mm/s) and Fe2 (0.54 mm/s). The asymmetric electron donation from terminal carboxylates provides a reason for this feature, with Asp-84 being closer to Fe1 and Glu-204 being anti, pointing away from Fe2, with other induction effects being similar. The only other strongly asymmetric isomer shifts (0.54/0.58 mm/s) are seen in **013**, which also has a syn-anti structure.

bidentate on Fe1, compensating the loss of Glu-238. As will be clearer when considering the "**w**" models, opening of the structures tends to lower isomer shifts.

Interestingly, among energetically viable candidates, one structure, **07**, displays isomer shifts in the range expected for P′, showing that such observed isomer shifts can indeed arise from a peroxo-type intermediate, if this intermediate has an open structure. The isomer shift of **07** is lowered by being both open *and* anti-anti. Different coordination modes of O_2 also give rise to both regimes of isomer shifts, confirming that one main determinant of the changed effective oxidation states of iron are the conformations of the carboxylates.

Hydrated (H_2O) Models: *J*-Coupling Constants and Isomer Shifts. *J*-Coupling Constants. As discussed above, among the water adducts, **w1** and **w2** displayed favorable free energies and had O−O stretch frequencies consistent with the experimental data. The main observation here is that the coupling now falls in a range from -184 cm^{-1} to -266 cm^{-1} for the four water-bound μ-1,2 structures, showing that water binding tends to increase the magnetic coupling by a modest amount.

Mössbauer Isomer Shifts. As seen in Table 2, among the four hydrated μ-1,2 structures, three of them (**w2**, **w3**, and **w4**) fall between 0.47 and 0.57 mm/s, while for **w1** it is 0.70 mm/s for both irons, similar to the 0.66 mm/s seen in its nonhydrated counterpart **01**. Thus, the Mössbauer isomer shifts correlate with the opening of the structures upon water binding, and again the two groups of isomer shifts are very distinct and similar to those seen for the "**0**" models. Models **w10** and **wFe2** have large isomer shifts and open structures. This suggests that peroxo intermediates with a μ-η^2,η^2 structure are less sensitive to changes in the remaining ligands. Furthermore, binding of water to Fe2 in **wFe2** where Glu-204 is anti and Asp-84 remains syn does not lead to a significant change in donated electron density to the irons. These species are not expected to be on the reaction coordinate of RNR.

Of particular interest is the comparison of the hydrated models, **w1** and **w2**, which are candidates for a stable peroxo intermediate. The fact that they are of similar free energy suggests that upon water binding, opening of the structure is thermodynamically feasible. It can be seen that **w2**, in comparison to **w1**, has lower isomer shifts reflecting decreased electron density on irons, due to opening of the structure in terms of Glu-238 reducing electron density on Fe1, and Glu-204 going from syn to anti, reducing the coordination numbers on both irons from 6 to 5.

These observations together with the results for the "**0**" models, imply that opening of the structure and/or syn-to-anti turning of Glu-204 correlate with lower isomer shifts. Importantly, both these structural changes are observed in the deoxy vs met structures and must occur along the reaction coordinate.

Hydrated ($OH^- + H^+$) Structures: *J*-Coupling Constants and Isomer Shifts. *J*-Coupling Constants. Models **h1**−**h4** and **h10** have open structures, because the protonation of Glu-238/O_2 forces the Glu-238 carboxylic residue to dissociate from Fe1. Computed *J*-coupling constants for these structures span a range similar to what has been observed above. The most interesting structure from the point of view of free energies and stretch frequencies is **h1**. It can be seen that this species has very weak coupling now with the proton in the bridging region; the computed J is $+11$ cm^{-1}, that is, weakly coupled.

Mössbauer Isomer Shifts. From Table 2, all four μ-1,2 structures (**h1**−**h4**) with a hydroxide and a proton bound to the site have isomer shifts in the lower range of 0.46−0.56 mm/s, agreeing well with our general observation that lower isomer shifts correlate with opening of the structure, as seen in the water adducts. The μ-η^2,η^2 structure **h10** exhibits intermediate isomer shifts of 0.56 and 0.60 mm/s, which agrees with the larger isomer shifts observed for this coordination mode in its corresponding structures **010** and **w10**.

When considering also the hydroxide forms of the water adducts, we envisioned that protonation/H-bonding to of O_2 could help activate oxygen by favoring the Fe(III)−O_2^{2-}−Fe(III) over the Fe(II)−O_2−Fe(II) resonance form. The control over these two resonance forms appears crucial to distinguish oxygen activation from the reversible binding that occurs in hemerythrin. Going from **w1** to **h1**, we do see a lowering of the isomer shift of ca. 0.15 mm/s from 0.70 mm/s, while creating an asymmetry between the iron sites (0.56/0.53 mm/s). This is caused by proton transfer to Glu-238 and/or O_2, which causes Glu-238 to dissociate from Fe1, opening the structure and reducing the coordination number of Fe1 from 6 to 5. A similar trend in isomer shift is observed experimentally in going from P to P′.[32] Furthermore, partial protonation of O_2 weakens the O−O bond as reflected in the O−O stretching frequency which decreases from 930 cm^{-1} in **w1** to 851 cm^{-1} in **h1**. Thus, compared to both **01** and **w1**, the O−O bond is activated in **h1** and **w2**. Interestingly, this weakening of the O−O bond correlates with an increase in the Fe−Fe distance upon opening of the bridge (see Table S4, Supporting Information). The Fe−Fe distance is 3.39 Å in **01**, 3.51 Å in **w2**, 3.77 Å in **07**, and 4.00 Å in **h1**.

Proton only Models: *J*-Coupling Constants and Isomer Shifts. *J*-Coupling Constants. The *J*-coupling constants of the viable **p**-candidates (**p1*Acs**, **p1*Aos**, **p1*Ao′s**, **p1*Aca′**, **p1*Bca′**, **p1*Aoa**, **p1*Aca** and **p1*Bca**, that is, when the terminal carboxylate is protonated and the bridge is closed) are in the range of -374 to $+12$ cm^{-1}. As the viable **p**-candidates are only relevant to P′ (*vide infra*) and there is no experimental estimate for the exchange coupling in P′, these values are not considered further.

Mössbauer Isomer Shifts. For **p1Acs**, **p1Bcs**, and **p1*Bcs**, protonation of the peroxide leads to O−O bond cleavage and low isomer shifts (0.24−0.37 mm/s). This reflects the associated higher oxidation states of the irons resulting from O−O cleavage. Similar low isomer shifts are observed in intermediate Q from MMO.[62] For **p**-structures with intact O−O bonds **p1*Bos**, **p1*Bo′s**, and **p1*Boa** are excluded due to high free energy or requiring a large structural rearrangement. The remaining **p**-candidates (i.e., closed structures with protonated terminal carboxylates) have isomer shifts in the range of 0.51 to 0.60 mm/s suggesting possible candidates for P′.

Absorption Profiles for Peroxo Candidates. There are experimental UV−vis data available for several peroxo-like intermediates in RNR proteins.[22,28,32] In order to further characterize the geometry-optimized intermediates in Table 2, we have computed their UV−vis spectra as described in the Methods section. We anticipate rather large errors in the computed spectra of the models, in particular the intensities, which are derived from oscillator strengths with errors of several orders of magnitude.[63] The largest error in computed benchmark absorption spectra was 4000 cm^{-1} (Figure S7, Supporting Information) for the oxo bridged diferric site. These errors are similar to typical errors reported for TDDFT ∼3000 cm^{-1}.[42,64]

(62) Lee, S. K.; Nesheim, J. C.; Lipscomb, J. D. *J. Biol. Chem.* **1993**, *268*, 21569–21577.
(63) Seth, M.; Ziegler, T. *J. Chem. Phys.* **2006**, *124*, 144105.
(64) Grimme, S.; Neese, F. *J. Chem. Phys.* **2007**, *127*, 154116.

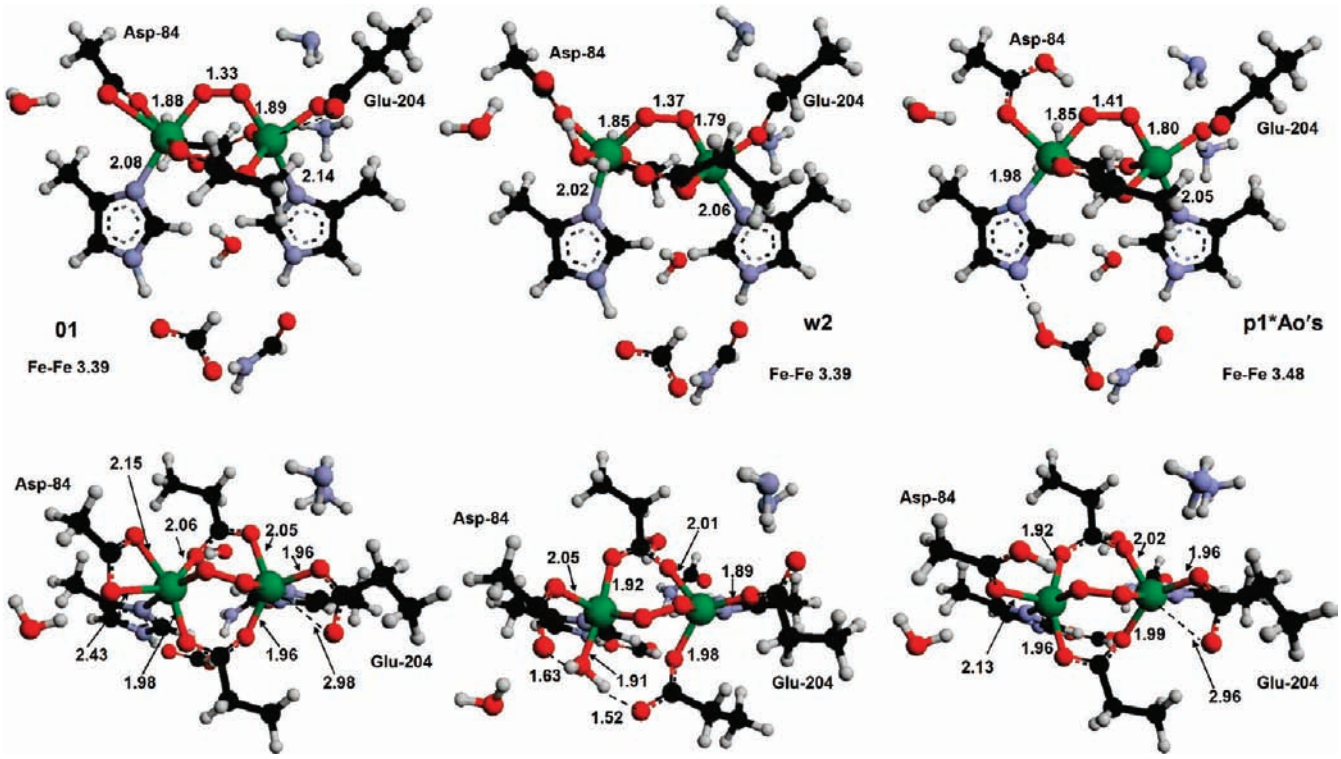

Figure 4. Optimized structures of models **01** (left), **w2** (middle), and **p1*Ao′s** (right). All distances are in Å.

In addition, the relative effect of shifting intensity upon protonation of the bridging ligand showed that such perturbations can indeed give rise to changes in the spectra and are well modeled by TDDFT. Furthermore, shifts in the profiles are expected to be substantially more accurate and can be used to correlate with the experimental absorption spectra. Calculations to calibrate the TDDFT are presented in the Supporting Information and show that there is an overemphasis on intensity derived from carboxylate to Fe^{III} CT, but observed changes in overall intensity among structures are valid.

The maxima in the computed spectra are listed in Table 2 in units of 10^3 cm^{-1}. The main observation is that the experimental maxima at 14 000−15 000 cm^{-1} and above 25 000 cm^{-1} for P in RNR mutants[22,28,29] and in Δ^9D[27] are well reproduced in **01** with maxima at 17 000 cm^{-1} and 23 000/26 000 cm^{-1}. The other peroxo intermediate candidate, **04**, has the same computed features in the absorption profile, but with half intensity at 17 000 cm^{-1}. Conversely, **w1** has peaks at 26 000 cm^{-1}, 20 000 cm^{-1}, 14 000 cm^{-1}, and 10 000 cm^{-1} not well resembling the observed spectrum of P. As its *J*-coupling constant was also out of the anticipated range, **w1** is not a realistic model for P.

The spin orbitals involved in the most intense transitions of **01** are shown in Supporting Information, Figure S3, and the composition (the two dominant configurational excitations) of the transitions is given in Table S3, Supporting Information. This analysis suggests that the peak at high energy (23 000 cm^{-1}) consists of a mixture of Asp-84 to Fe1 excitations and O_2 to Fe2 excitations, i.e. the peak arises from several LMCT excitations in that energy regime involving both irons. On the other hand, the characteristic transition at 700 nm (14 300 cm^{-1}) in typical P intermediates (see Table 1) corresponds to our computed peak at 17 000 cm^{-1}. Analysis of the spin orbitals involved reveals that this peak again comes from a mixture of configuration excitations. While the contribution to this transition reflects too much carboxylate to Fe CT mixing (based on resonance Raman studies[32]), the contribution with the largest oscillator strength in this region (0.013) involves typical O_2-to-Fe CT excitations, for example, 124α → 133α and 130α → 136α (Table S3, Supporting Information). 124α is the vertical π^* orbital of peroxide, transferring charge to 133α, which is a mixture of the vertical π^* and Fe 3d (both d_σ and d_π as seen in Figure S3, Supporting Information, which derives from the twisted Fe−O bonds in the peroxo intermediate); 130α → 136α is clearly a O_2^{2-} π^* to Fe1-d_π CT excitation.

The change in the observed absorption spectra when going from intermediates P to P′ is considered below.

Discussion

Implications for P. The structure of **01** is closed, indicating that Glu-115 and Glu-238 both bridge the irons. Model **01** has coordination numbers of 6 for Fe1 and 5 for Fe2 with syn conformations for both the terminal carboxylates. The free energy of this model is the lowest of any nonprotonated structure in this study (−19.5 kcal/mol) and all computed properties are in good agreement with known experimental data for P. In order to test the sensitivity of altered coordination numbers on this promising candidate, we reoptimized a structure of **01** with coordination numbers 5 for both irons. This structure, referred to as **01(5,5)** had a free energy of −19.7 kcal/mol, essentially identical to **01**. Apart from the change in coordination of Asp-84 (bindentate in **01** and monodentate in **01(5,5)**), the structures are very similar. We thus consider both forms as viable candidates for P; the 6,5 model for P trapped by the D84E variant and the 5,5 isomer for P in WT RNR. However, as data are available for the mutants only, we have correlated experimental data with **01** and not **01(5,5)**, recognizing that the latter models the active state of P in the WT protein.

The structure of **01** is shown in detail in Figure 4. It resembles well the earlier suggested structure of P in D84E RNR[29] in terms of the μ-1,2 coordination mode of O_2 and the closed structure of the intermediate. All essential metal−ligand bond lengths and the conformations of carboxylates are similar, as well as

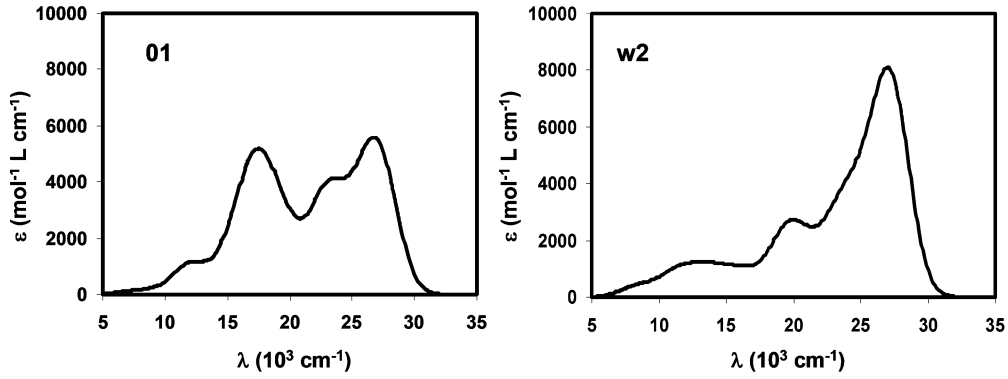

Figure 5. Computed UV−vis absorption profiles from TD-DFT of **01** (left) and **w2** (right).

the coordination geometry of O_2: The previously deduced O−O bond was 1.32 Å, with Fe1−O_A = 1.91 Å and Fe2−O_B = 1.93 Å. In **01**, O−O = 1.32 Å, Fe1−O_A = 1.88 Å, and Fe2−O_B = 1.89 Å.

Importantly, the computed properties of the (6,5)-coordinated form of **01** are all in good agreement with experimentally observed data for comparable peroxo intermediates, shown in Table 1: (i) The Fe−O and O−O stretch frequencies of **01** are 447 cm^{-1} and 957 cm^{-1}, respectively, similar to the 457 cm^{-1} and 868 cm^{-1} found for the P intermediate in the W48F/D84E mutant;[29] ii) the exchange coupling constant is slightly negative (−63 cm cm^{-1}), implying weak antiferromagnetic coupling as has been found from Mössbauer spectroscopy studies of the same mutant (−50 cm^{-1});[35] the computed isomer shifts of 0.66 mm/s for both Fe1 and Fe2 in **01** are in agreement with all P-type intermediates in RNR proteins listed in Table 1 (ranging from 0.61 to 0.66 mm/s); and finally, the peaks in the computed absorption profile of **01** at 17 000 cm^{-1} and 23 000/26 000 cm^{-1} are similar to the experimentally observed maxima at 14 000−15 000 cm^{-1} and 25 000 cm^{-1} for P in RNR mutants[22,28] and in Δ^9D.[27] The good agreement of our model **01** with the experimental data observed in the mutants suggests that Glu-84 is bidentate in the D84E mutant P intermediate. Whereas **01** is clearly a good candidate of P observed in the mutants, the computed **01(5,5)** structure with coordination number 5 for both irons (i.e., Asp-84 is monodentate) would exist in the WT, supported by its competitive free energy of −35.1 kcal/mol. Because of its lower coordination number to iron, it has lower isomer shifts (0.58/0.57 mm/s) and Fe−O and O−O stretches of 416 cm^{-1} and 1047 cm^{-1}, respectively. A main difference is that the monodentate Asp-84 in the WT computed model **01(5,5)** allows for water (or OH^- + H^+) to bind to Fe1 or for the carboxylate to be protonated, yielding the new intermediate P′. Thus, this structure (**01(5,5)**) would appear to be mechanistically important as the active WT-conformation of P.

Implications for P′. We now consider the intermediate P′,[32] recently observed in the W48A/Y122F mutant, which goes on to form X in a chemical rescue experiment with 3-methyl indole.[65] Two experimental observables define this intermediate relative to P. Decreased UV−vis intensity at 15 000 cm^{-1} and a change in Mössbauer isomer shifts from ∼0.63 mm/s to distinctly smaller isomer shifts interpreted as either two symmetric species having 0.52/0.52 and 0.45/0.45 mm/s, or two species with 0.60/0.45 mm/s and 0.43/0.43 mm/s.[32] Similar spectral features have been observed in a peroxo intermediate in ToMO.[34]

From the studies above, the cis μ-1,2 peroxy bridged structure **01(5,5)** is the only viable candidate for intermediate P in WT. Three possibilities for the conversion of P to P′ are: (1) that **01(5,5)** (i.e., P in WT) directly rearranges; (2) the addition of a water (possibly dissociating to OH^- and H^+) and (3) direct proton donation. The only viable candidate for the first option from Table 2 is **07** (noting that this would have to be the minor component of P′, as there is still significant intensity at 15 000 cm^{-1} in the TDDFT spectrum for this species, Figure S4, Supporting Information). However, Model **07** is open and anti-anti. This requires that Glu-238 now binds Fe2 in a bidentate fashion, and thus a large structural rearrangement would be involved upon conversion of **01(5,5)** to **07**. This coupled with the 9.3 kcal/mol increased energy of this species would lead to a large energy barrier between P and P′ which is inconsistent with the estimated kinetics (400 to 4000 s^{-1}) ruling out **07** as a candidate for P′.

Water addition to P. We have found that a number of computed structures exhibit isomer shifts in the range observed for P′. Among these, the only energetically competitive ones are **w2** (δ = 0.51/0.47 mm/s; ΔG = −3.9 kcal/mol); **w4** (δ = 0.57/0.56 mm/s; ΔG = −10.0 kcal/mol); and **h1** (δ = 0.56/0.53 mm/s; ΔG = +1.4 kcal/mol). Thus, the observed 'unusual' isomer shifts[32] can be achieved by opening the structure of the peroxo intermediate (i.e., loss of one carboxylate bridge).

In **w2** and **h1**, these structural changes correlate with oxygen activation because the irons have more ferric character and the O−O bond weakens, reflected in the ca. 100 cm^{-1} decrease in ν_{O-O} relative to **01**. It is therefore reasonable to consider these structural correlations to be consistent with the conversion of P to P′.

The bleaching of the UV−vis absorption at 14 300 cm^{-1} is the other experimental difference between P and P′. Comparing the absorption profiles to that computed for **01**, in all these three models, the relative intensity of the peak at ca. 15 000 cm^{-1} is much smaller, compared to that at ∼25 000 cm^{-1}. However, only in **w2** is this feature bleached. Still, the change is significant in all three complexes and also correlates with the opening of the structure. *Thus, in this pathway, weakening of the transition at ∼15 000 cm^{-1} correlates with water binding and opening of the structure.* The computed spectrum of **w2** is in best agreement with the experimental data and may be the species responsible for the observed absorption spectrum.[32] However, **w4**, or **h1** could correspond to the second componenspond to the second component of P′ observed in the Mössbauer studies. The computed spectra of **01** and **w2** are compared in Figure 5.

(65) Saleh, L.; Kelch, B. A.; Pathickal, B. A.; Baldwin, J.; Ley, B. A.; Bollinger, J. M., Jr. *Biochemistry* **2004**, *43*, 5943–5952.

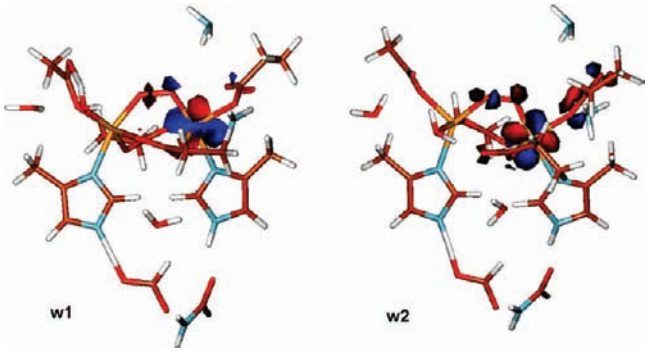

Figure 6. The HOMOs of the reduced closed and open water adducts **w1** (left) and **w2** (right).

The orbital analysis in Table S5 (Supporting Information) suggests that bleaching in P′ is due to a substantial decrease in O_2^{2-}-to-Fe^{III} CT intensity and simultaneous increased intensity of the remaining carboxylate excitations. The large decrease of this peak in the computed absorption spectrum of **w2**, compared to **01**, can explain the experimentally observed bleaching in P′ as due to water binding, opening of the Glu-238, and reorientation of Glu-204 into the *anti* conformation.

From the optimized geometric data (see Figure 4 and Table S2, Supporting Information), it can be seen that the O−O bond increases from 1.32 Å in **01** to 1.37 Å in **w2**, consistent with activation of O−O. The Fe−O bonds decrease correspondingly. The vibration frequencies confirm these observations, with ν_{O-O} decreasing from 957 to 842 cm^{-1} and a small (6 cm^{-1}) increase in ν_{Fe-O} (see Table 2). The isomer shifts are lowered by 0.15−0.19 mm/s.

The change in carboxylate conformations may help to activate the site for the generation of X. The critical step from P to P′ (i.e., closed to open and Glu-204 syn-to-anti) in this possible model appears to activate the diiron site for electron transfer from Trp-48. This hypothesis can be tested by considering the relaxed electron affinities (EA) of the computational models. These values have been included in the seventh column of Table 2, and reflect the energy of adding an exogenous reducing electron to the structures and reoptimizing the geometries. Interestingly, the candidates for P′ have higher EAs than **01**. In particular, our favored water candidate, **w2**, has an EA of 74.0 kcal/mol, whereas that of **01** is 64.9 kcal/mol, a difference of 9.1 kcal/mol. The reason for the increased EA of the open water adduct **w2** is best seen by comparison to **w1**, which has a water-bound, closed structure (Figure 6). The HOMO of the reduced state is mainly localized on Fe2, but for the open **w2** structure this is delocalized over Glu-204, reducing electronic repulsion and lowering the calculated energy of the HOMO from +2.31 eV in **w1** to +2.01 eV in **w2**.

The structures of **01** and **w2** with relevant interatomic distances are compared in Figure 4. The coordination mode of the terminal carboxylates may rearrange with small barriers at room temperature, as energy differences between conformations are expected to be small.[18] The most significant differences are the bound water, the opening of the structure, and the 120° rotation of the Fe−O−C−O dihedral angle of Glu-204, caused by electrostatic repulsion between the negatively charged Glu-238 and Glu-204, leading to the anti conformation as seen experimentally in the met crystal structure.

In summary, the observed changes in O−O stretching frequency directly imply that the **w2** state has a weaker O−O bond and slightly more oxidized irons (as seen in the isomer shifts). The conversion of **01** to **w2** increases the EA (by 9 kcal/mol relative to **01** and by 3 kcal/mol relative to **01(5,5)**), possibly a means to trigger ET from Trp-48. However, other mechanisms can be envisioned, for example, **h1** converting to X, if **h1** is the reactive species of P′. The Mössbauer spectrum of P′ indicates that two species exist, potentially with one form being reactive. Thus, we have identified two structures (**w2**, **h1**) that can explain the observed data for P′, and suggested them to play an important mechanistic role in activating the site for reduction in the water pathway. The increase in EA from P (**01**) to P′ (**w2**) of 9.1 kcal/mol (Table 2) may imply that a threshold has been reached for reduction by Trp-48 to form X. The lowered isomer shifts and a 0.3 eV decrease in HOMO energy of the reduced states of **01** vs **w2** support this idea. However, the details of further reaction (i.e., PCET) has to be studied for insight into the formation of X from this model of P′.

Proton Addition to P. Stable structures were found with the proton on a carboxylate that H-bonds to the peroxide. Model **p1*Bos** is the singular example of the H^+ bound to previously bridging carboxylate, this model is significantly less stable (−26 kcal/mol) than all others and excluded. Models **p1*Bo′s** and **p1*Boa** resulted in a geometry where the formally bridging carboxylate rotates such that the proton is located between this and the terminal carboxylate bound to Fe2. Such a structure would require a large reorganization energy and is not consistent with the kinetics of the P to P′ conversion. The remaining structures either have the proton on the terminal Asp or terminal Glu and H-bonding to peroxide, and they can be grouped into three sets as discussed below.

Models **p1*Aos**, **p1*Aca′**, and **p1*Aoa** are iso-energetic (free energies between −43.3 and −43.9 kcal/mol), with closed structures after optimization with protonation of Asp-84 that has an H-bond to O_A. The Fe1−O_A distance is 1.97−1.98 Å, the Fe2−O_B distance is 1.94 Å, and the O−O distance is 1.35−1.36 Å. The isomer shifts of 0.58−0.59 mm/s are slightly larger that the rest of the **p**-structures, correlating with the stronger O−O bond, as also seen in the computed O−O bond stretch frequencies of 945−964 cm^{-1}. The reduction in these isomer shifts is modest compared to the reference P structure (**01**), implying that less electron density has been transferred to O_2, i.e. these peroxides are less activated, compared to the "**w**" and "**h**" structures above. All these structures have a calculated absorption feature at essentially the same energy (16 000 vs 17 000 cm^{-1}) and intensity ($\epsilon \approx$ 5000−6000 L $mol^{-1}cm^{-1}$) as the peroxo-to-iron LMCT band of **01**, Figure S4, Supporting Information. Thus, bleaching of the LMCT band has not been achieved in these structures where the O−O bond remains similar to that of P. The negligible bleaching and modest decrease in isomer shifts correlates with the lack of activation of the O−O bond and is not consistent with experimental data on P′.

Models **p1*Acs**, **p1*Ao′s**, and **p1*Aca** optimized to highly similar, closed structures with syn conformation of both terminal carboxylates, protonation of Asp-84 with a H-bond to O_A (2.51−2.52 Å), and with the Glu-204 monodentate. The free energies are very similar (−45.4 to −46.1 kcal/mol). The Fe1−O_A distance is ∼1.85 Å, Fe2−O_B = 1.80−1.81 Å, and O−O = 1.41 Å. The isomer shifts (0.52−0.55 mm/s) are consistent with P′, as is the bleaching observed in the computed absorption spectra at 15 000 cm^{-1}: Now, the peak is at 13 000 cm^{-1} and has decreased in intensity by ∼1500 L mol^{-1} cm^{-1}, Figure S8, Supporting Information. The computed O−O stretch frequency is 724−727 cm^{-1}, consistent with an elongated O−O bond. We see that the bleaching clearly correlates with activation of the O−O bond, as also observed in the hydrated P′ candidate **w2**; thus, the experimental observed data can be correlated to O−O bond activation in both models. H-bonding to the peroxide localizes the electron density on this ligand and increases the Z_{eff}. This larger Z_{eff} reduces the isomer

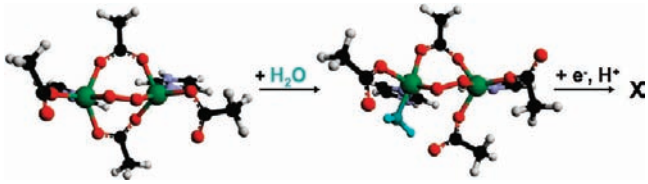

Figure 7. Suggested water mechanism of O_2 binding and activation in class I ribonucleotide reductase.

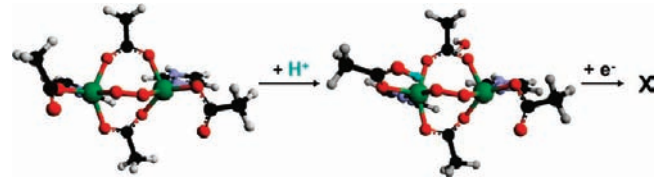

Figure 8. Suggested exogenous protonation mechanism of O_2 binding and activation in class I ribonucleotide reductase.

shifts and shifts the LMCT band. These structures are consistent with the experimental data for P′ and the structural parameters of **p1*Ao′s** are included on the right side of Figure 4.

Models **p1*Bca′** and **p1*Bca** converged from structures with oxygen B protonated and have Glu-204 protonated with a hydrogen bond to O_B, and an O−O bond of 1.41 Å analogous to **p1*Acs**, **p1*Ao′s**, and **p1*Aca** where the Asp on Fe1 is protonated and H-bonds to O_A of the peroxide. Spectral bleaching is also observed in these structures, Figure S9, Supporting Information. However, the isomer shifts (0.58−0.60 mm/s) have not decreased as much as when Asp-84 is protonated. This set of models shows that protonation of the terminal carboxylate on either side of the site with an intact, closed structure can result in the spectral features of P′.

Mechanism of O_2 Activation in RNR. We have identified **01** as the most likely structure of P in the D84E mutants and the equally stable **01(5,5)**, which is similar to **01**, except it has a coordination number of 5 also at Fe1, as the likely active form of P in the WT enzyme. From these results there are two viable reaction pathways from P: (1) water addition to Fe1 causing opening of Glu-238, increasing the EA and activating the site for PCET to form X, and (2) H^+ addition to a terminal carboxylate (in a closed structure), increasing the EA and triggering a subsequent ET to form X.

In the first pathway, the available open coordination site on Fe1 would allow water to bind, and this would give an intermediate (**w2**, which could dissociate into **h1**) with properties in agreement with experimentally observed data on intermediate P′.[32] Water binding to **01(5,5)** requires a free energy of 16 kcal/mol to give **w2**. These two structures (**w2** and **h1**) may exist in equilibrium, as they are isoenergetic. Given an uncertainty estimate of 10 kcal/mol, a barrier of 6 kcal/mol or more is expected for water binding, and such a barrier could be consistent with the 400−4000 s^{-1} rate of converting P into P′ in the W48A/Y122F mutant.[32] In the WT, the barrier likely remains as the iron sites of the W48A/Y122F mutant and WT should be similar, but in the WT the P′ is immediately converted to X upon ET.

Based on these results for **w2**, water binds by displacing Glu-238 from bridging to Fe1. This leads to an open structure where Glu-238 electrostatically repels Glu-204, which moves into an anti conformation as seen in the **w2** structure. Importantly, these structural changes correlate with the experimentally observed changes between the deoxy and met states.[14,15] Additionally, ENDOR results suggest the presence of a water derived oxygen in addition to those from O_2 in X.[66]

The suggested intermediates **01(5,5)** and **w2** are shown in Figure 7 for the water reaction coordinate of oxygen activation leading to X. Note that water binding increases the EA by ∼5 kcal/mol activating ET from Trp-48 which would likely be coupled to proton transfer due to reasons of charge neutrality.

(66) Burdi, D.; Sturgeon, B. E.; Tong, W. H.; Stubbe, J.; Hoffman, B. M. *J. Am. Chem. Soc.* **1996**, *118*, 281–282.

The second possible pathway for the formation of P′ is the addition of a proton to P, Figure 8. This is highly exergonic by ∼25 kcal/mol and increases the EA of the site to ∼100 kcal/mol. The proton is formally on a terminal carboxylate and H-bonding to the proximal O of the peroxide causing the Fe−O bond to increase, activating the O−O for cleavage and causing bleaching of the optical spectrum. The two species experimentally observed in P′ could be two conformers with the H^+ on the same terminal carboxylate or could result from partial transfer of the proton to the other terminal carboxylate. In this scenario Glu-238 remains closed in P′ and water would add subsequent to X, opening the site.

From the energetics of these two mechanisms presented in Table 2, the H^+ pathway is favored, however the water path is still energetically accessible. Experimentally these can be distinguished by kinetic isotope effects on the P to P′ conversion or determining if a water is bound to the site in X.

In summary, intermediate P trapped in the D84E variant of RNR is well-defined as a cis-μ-1,2 peroxo bridged closed structure with a bidentate terminal carboxylate on Fe1 which inhibits conversion to P′. In WT this Asp is monodentate and could either accept a H^+ or allow water to bind to the now open coordination position at Fe1 to generate P′. P′ is activated for reduction (by Trp-48) by its increase in EA either associated with protonation of a terminal carboxylate which is most energetically favorable, or by water coordination which opens the site and decreases the carboxylate charge donation to the irons. The major difference between these possible reaction pathways is whether the water binds and opens the bridge before or after formation of X.

Acknowledgment. We thank Prof. J. M. Bollinger for insightful discussion. We acknowledge grants from the Danish Natural Science Research Council, 272-07-0030 (K.P.J.), the Villum-Kann Rasmussen Foundation (K.P.J.), Danish Center of Scientific Computing, CPU-0107-05 (K.P.J.), and the Natural Science Foundation, MCB 0919027 (E.I.S.).

Supporting Information Available: Models computed for obtaining the correlation equation for isomer shifts (Table S1), figure of the corresponding fit (Figure S1), the structure of the geometry optimized deoxy state (Figure S2), optimized bond lengths (Table S2), optimized spin orbitals involved in transitions of **01** (Figure S3), most important transitions of **01** (Table S3), computed absorption profiles from TD-DFT (Figure S4), relative electronic energies computed with various model setups (Table S4), geometry optimized structures of full computational models (Figure S5), comparison of experimental and computed met state structure (Figure S6), computed met absorption spectrum with and without a proton on the oxo bridge (Figure S7), test-calculations of isomer shifts (Table S5), computed absorption spectra of **p**-models (Figure S8), computed bleaching of p-candidates (Figure S9). This material is available free of charge via the Internet at http://pubs.acs.org.

JA809983G